Doctoral Dissertation

Mechanism analysis in pattern formation of negative type photoresist using novel quantum yield measurement and quartz crystal microbalance method

Asuka Kimura

July 2018

Graduate School of Engineering,
Osaka University

Mechanism analysis in pattern formation of negative type photoresist using novel quantum yield measurement and quartz crystal microbalance method

（新たな量子収率測定方法と水晶振動子マイクロバランス法を用いた
ネガ型フォトレジストのパターン形成におけるメカニズム解析）

July 2018

Asuka Kimura

Department of Applied Chemistry

The Graduate School of Engineering

Osaka University

Preface

The study of this thesis has been carried out under the supervision of Professor Takahiro Kozawa (Osaka University), Professor Shu Seki (Kyoto University) and Associate Professor Kentaro Taki (Kanazawa University).

The object of this thesis is to accurately understand the photo-curing process and the dissolution process of negative resists during development using novel quantum yield measurement and quartz crystal microbalance method.

A. Kimura

Asuka Kimura

Department of Applied Chemistry

Graduate School of Engineering

Osaka University,

Asuka Kimura

Japan

July 2018

Contents

General Introduction

Photosensitive imaging materials, called photoresists, have been widely used for manufacturing electronic devices such as displays and semiconductors.[1–3] Depending on a response to light, photoresists are classified as a positive- or negative-type. Positive- and negative-type photoresists become soluble and insoluble in the developer after exposure to light, respectively (**Fig. 1**).

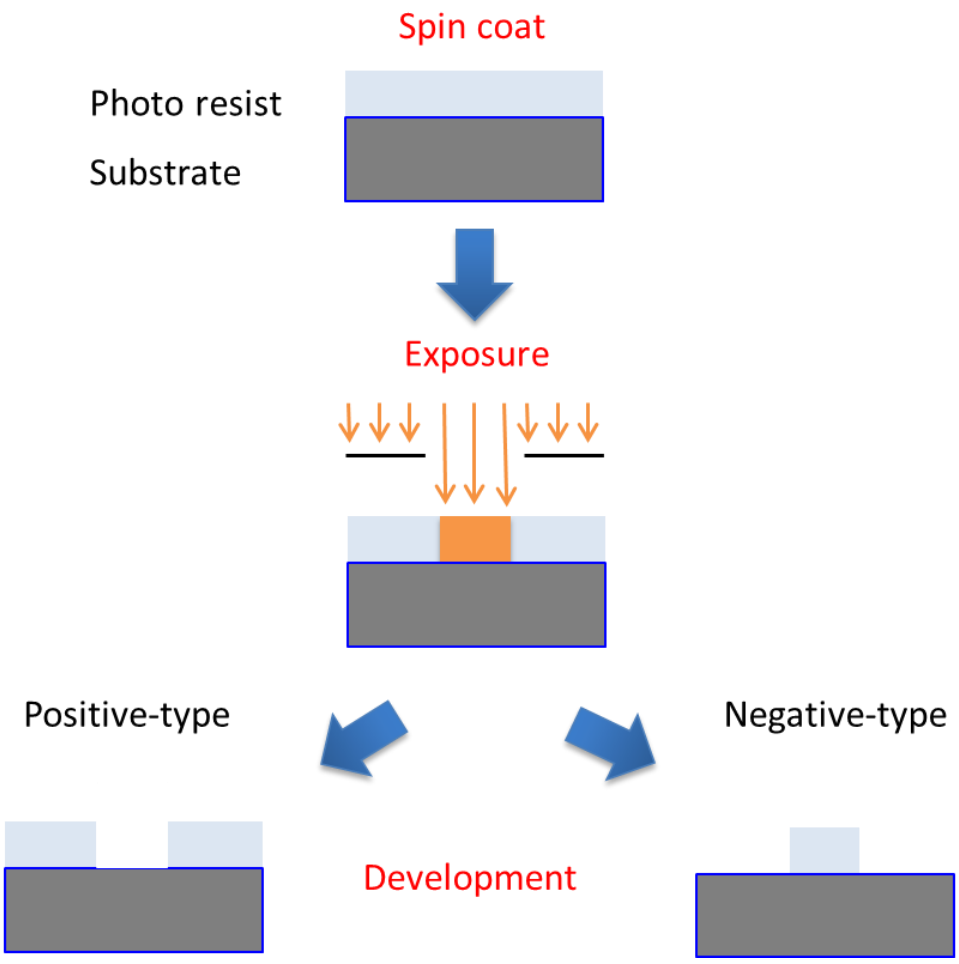

Fig. 1. Lithographic imaging process.

The positive-type photoresists are generally prepared in the presence of photoacid generators, which decompose to generate acids for the pattern formation upon exposure to light. The most famous positive-type photoresist utilizes the photoreaction of 1, 2-naphthoquinone-diazido-5-sulfonic acid ester and phenolic resin (**Fig. 2**). The generated acids dissolve with the novolak resin in an alkaline aqueous solution. Positive-type photoresists have been widely used in high-volume production lines of semiconductor devices such as memories and logics. In the current high-volume production lines, a highly sensitive resist, called a chemically amplified resist, has been used. The chemically amplified resists also utilize the photoacid generators. In these resists, the generated acids catalyze the deprotection of partially protected polymers during the post-exposure baking to induce the polarity change of the polymers.

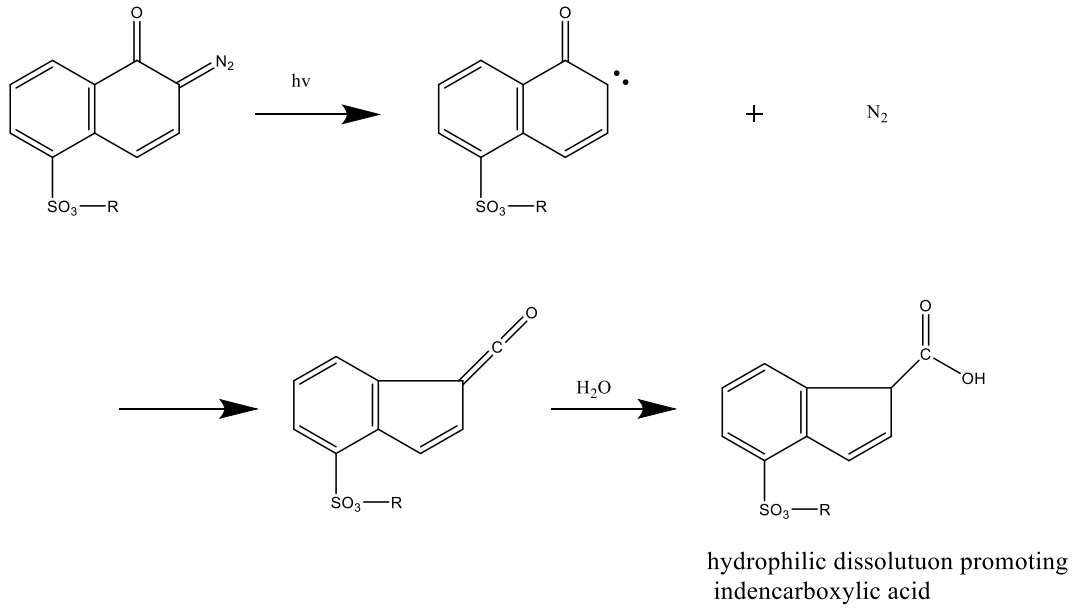

Fig. 2. The photoreaction of 1,2-naphthoquinone-diazido-5-sulfonic acid ester.

The negative-type photoresists generally utilize the radical polymerization. In this thesis, the negative resist is focused on and the sensitization process and its reaction mechanism are explained in details. The negative-type photoresist is composed of the monomer, the photo-radical initiator, and the polymer which has both a soluble unit in alkaline aqueous solution and crosslinking unit. When the photo initiators are irradiated by light, the initiator radicals are generated. The generated initiator radicals react with monomers to produce monomer radicals. Finally, the monomer radicals react with the polymers to crosslink the polymers (**Fig. 3**). The crosslinked polymers are insoluble in the developer. The pattern imaging of a negative resist utilizes the insolubilization of the photocured part and the dissolution of the uncured part in the developer.

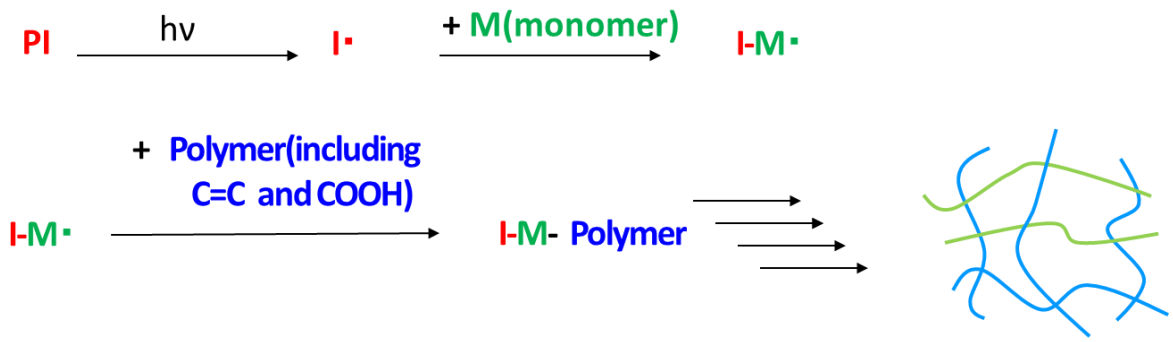

Fig. 3. The radical polymerization of negative-type resists.

The negative-type resists have been widely used as color filters, black matrix, photo spacers, banks, and overcoats in high-volume production lines of liquid crystal displays and organic light-emitting electroluminescence devices.[4,5)]

In the development of such photoresists, the photosensitivity is an important factor because it determines the throughput of production lines. In addition to the sensitivity,

the control of the resist shape after development is an another important factor for applying the photoresists to various fields. However, the pattern formation processes of the resist materials consist of multiple steps and each step is complicated. It is difficult to improve the resist formulation and molecular structures from the resist performance such as sensitivity, resolution, and pattern shape. The pattern formation processes consist of 4 steps (**Fig. 4**). The first step is the radical generation from photoinitiators upon exposure to light. The second step is the radical polymerization. The third step is the development in an alkaline aqueous solution. The final step is the bake of the obtained patterns.

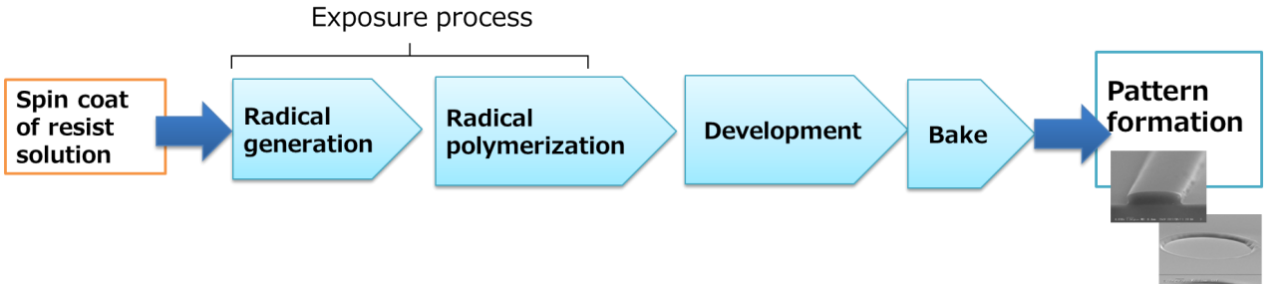

Fig. 4. The pattern formation processes of resist materials.

The aim of this thesis is to accurately understand the photo-curing processes and the dissolution processes of the negative resists during the development. Understanding the functional characteristics of materials in each step of the pattern formation of a negative resist is expected to contribute to the development of a high performance resist and an accurate resist shape simulator.

The mechanism analysis of the photo-curing process

The photo-curing process has been widely investigated because it significantly influences the resist sensitivity. This process consists of the radical generation from an initiator by UV irradiation and subsequent cross-linking. The parameters which affect the initiator sensitivity against UV light are the UV absorbance of the initiator, the radical generation efficiency of the initiator, and the reactivity of the radical with the monomer.

In the negative-type photoresists, it has been reported that the *o*-acyloxime ester compounds efficiently induce the polymerization of the acrylate monomers and unsaturated polyesters [6-14]. Regarding the photodecomposition process of an oxime type initiator, there are several reports on the radical generation mechanism. [15-19] The photoinduced pathways to radical generation of the oxime type initiators consist of two competing paths (depending on the substituents R): *E*/*Z* isomerization and fragmentation yielding radicals. The cleavage of the N−O bond yields iminyl and acyloxy radicals, which undergo further fragmentation or decarboxylation reaction (**Fig. 5**).

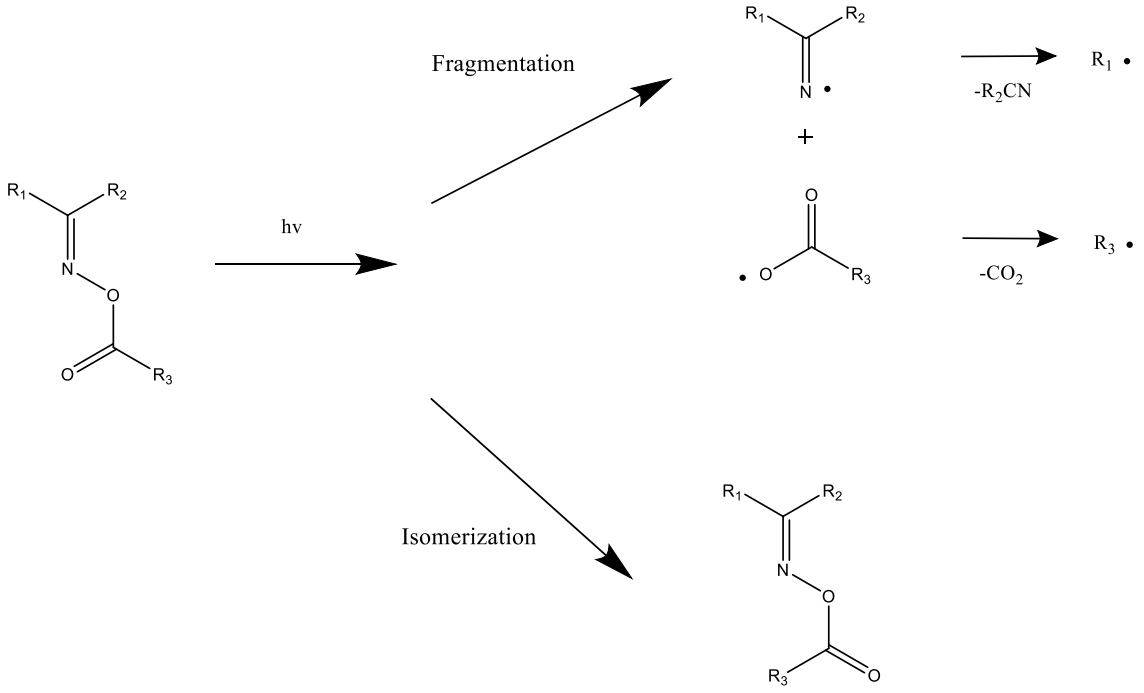

Fig. 5. Photoinduced reaction pathways of oxime esters.

However, there are few reports on the systematic comparison of the radical generation efficiency. Generally, an absorption change of the compound with respect to the amount of absorbed light is used as an indicator for determining the quantum yield of the initiator. The schematic of UV change used for the quantum yield evaluation of photoinitiator is shown in **Fig. 6.**

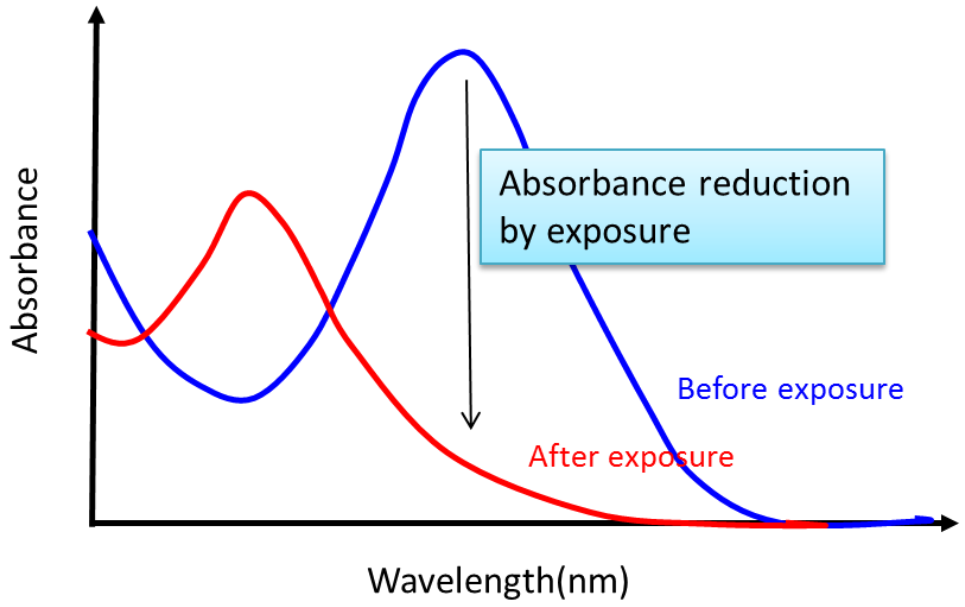

Fig. 6. Schematic of typical UV spectral change of photoinitiator.

However, since the absorption spectra do not change before and after irradiation for many oxime type initiators, the comprehensive analysis of quantum yields cannot be done using the conventional quantum yield measurement method.

Therefore, the author tried to develop a new method to estimate the quantum yield of the initiator, of which absorption spectrum does not change upon UV irradiation. The developed method utilizes a galvinoxyl radical (G) as a radical quencher. In order to understand the relationship between the quantum yield and the molecular structure of the initiator, quantum chemical calculations were carried out and the quantum yields obtained by measurements were compared with the calculation results. The radical generation efficiency is discussed in Chapter 1.

The mechanism analysis of the dissolution process

The dissolution processes have been widely investigated because they have a significant impact on the formation of the resist shape. In particular, the taper angle is considered to be closely related to the dissolution kinetics. **Fig. 7** depicts an assumption regarding the relationship between taper angle and dissolution rate.

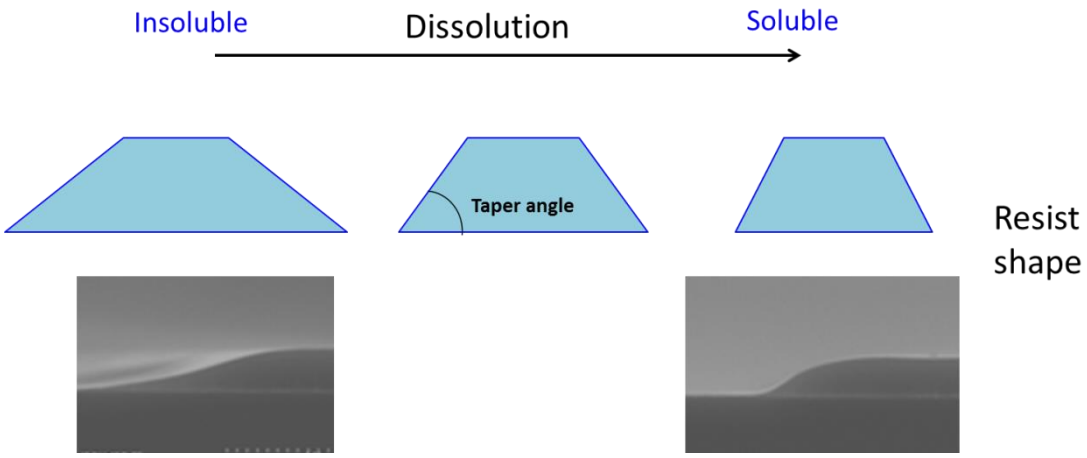

Fig. 7. Schematic of relationship between resist shape and dissolution in developer.

The dissolution behavior has been reported by a quartz crystal microbalance (QCM),[20-25] a high speed atomic force microscopy (AFM),[26-30] and other methods.[31-40] However, these studies mainly focused on the positive-type resist materials for manufacturing semiconductor devices. The studies on the dissolution kinetics of negative type resist materials for manufacturing displays were quite limited.[39]

In Chapter 2, the author investigated the development behavior of the negative type photoresist in a tetramethylammonium hydroxide (TMAH) aqueous developer solution to clarify the basic dissolution mechanisms of the negative-type photoresists used for

the display manufacturing. The negative-type photoresist is insolubilized upon exposure to UV light unlike the positive-type resist. Understanding the dissolution kinetics of unexposed polymer is essential to the resist design. After the elucidation of the dissolution kinetics of polymer itself, the effects of resist components on the dissolution kinetics of the polymer are discussed.

The analysis of relationship between the cross-linking in photo-curing process and the dissolution kinetics in the developer

In addition to the dissolution behavior of unexposed region, that of the weak photo-curing region also affects the resist shape (**Fig. 8**).

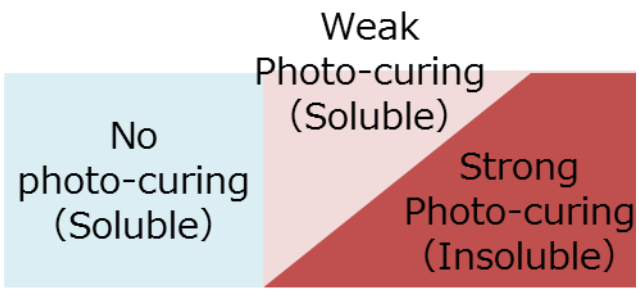

Fig. 8. Schematic of relationship between photo-curing and development.

The photo-curing processes have been investigated by IR spectroscopy,[40-42] Raman spectroscopy,[43] and other methods.[44-45] However, the details of the relationship between cross-linking in photo-curing process and dissolution kinetic in the developer are unknown. In Chapter 3, the author analyzed the development process of cross-linked photoresists. The C=C double bond conversion induced upon exposure to UV light was

measured using a real-time FTIR method. The dissolution behavior of exposed resists in TMAH aqueous developer was measured using QCM. The effects of cross-linking on the dissolution kinetics is discussed.

References

1) T. Tsuda, Displays **14**, 115 (1993).

2) R.W. Sabnis, Displays **20**, 119 (1999).

3) H. Ito, Advances in Polymer Science Series, Vol. 172, p. 37.

4) H. S. Koo, M. Chen, C. H. Kang, and T. Kawai, Jpn. J. Appl. Phys. **47**, 4954 (2008).

5) C. K. Lee, F. H. Hwang, C. C. Chen, C. L. Chang, and L. P. Cheng, Adv.Polym.Technol. **31**, 163 (2012).

6) D. Shiota, Y. Tadokoro, K. Noda, M. Shiba, and M. Fujii, J. Photopolym. Sci. Technol. **24**, 625 (2011).

7) C. J. Groenenboom, H. J. Hageman, P. Oosterhoff, T. Overeem, and J. Verbeek, J. Photochem. Photobiol. A **107**, 261 (1997).

8) F. Amat-Guerri, R. Mallavia, and R. Sastre, J. Photopolym. Sci. Technol. **8,** 205 (1995).

9) M. Yoshida, H. Sakuragi, T. Nishimura, S. Ishikawa, and K. Tokumaru, Chem. Lett. 1125 (1975).

10) P. Baas and H. Cerfontain, J. Chem. Soc. Perkin II 156 (1979).

11) P. Baas and H. Cerfontain, J. Chem. Soc. Perkin II 1653 (1979).

12) R. Mallavia, R. Sastre, and F. Amat-Guerri, J. Photochem. Photobiol. A **138**, 193 (2001).

13) Y. Miyake, H. Takahashi, N. Akai, K. Shibuya, and A. Kawai, Chem. Lett. **43**, 1275

(2014).

14) X. Allonas, J. Lalevée, J.–P. Fouassier, H. Tachi, M. Shirai, and M. Tsunooka, Chem. Lett. 1090 (2000).

15) Y. Muramatsu, M. Kaji, A. Unno, and O. Hirai, J. Photopolym. Sci. Technol. **23**, 447 (2010).

16) D. E. Fast, A. Lauer, J. P. Menzel, A.-M. Kelterer, G. Gescheidt, and C. Barner-Kowollik Macromolecules **50**, 1815 (2017).

17) G. A. Delzenne, U. Laridon, and H. Peeters, Euro. Polym. J. **6**, 933 (1970).

18) C. Dietlin, J. Lalevee, X. Allonas, J. P. Fouassier, M. Visconti, G. Li Bassi, and G. Norcin, J. App. Polym. Sci. **107**, 246 (2008).

19) J. V. Crivello and E. Reichmanis, Chem. Mater. **26**, 533 (2014).

20) W. Hinsberg, F. A. Houle, S. W. Lee, H. Ito, and K. Kanazawa, Macromolecules **38**, 1882 (2005).

21) W. D. Hinsberg, C. G. Willson, and K. K. Kanazawa, J. Electrochem. Soc. **133**, 1448 (1986).

22) M. Toriumi, T. Ohfuji, M. Endo, and H. Morimoto, J. Photopolym. Sci. Technol. **12**, 545 (1999).

23) H. Ito, IBM J. Res. Develop. **45**, 683 (2001).

24) A. Sekiguchi, J. Photopolym. Sci. Technol. **23**, 421 (2010).

25) K. J. Harry, S. Strobel, J. K. W. Yang, H. Duan, and K. K. Berggren, J. Vac. Sci. Technol. B **29**, 06FJ01 (2011).

26) T. Itani and J. J. Santillan, Appl. Phys. Express **3**, 061601 (2010).

27) J. J. Santillan and T. Itani, Jpn. J. Appl. Phys. **51**, 06FC06 (2012).

28) J. J. Santillan and T. Itani, Jpn. J. Appl. Phys. **52**, 06GC01 (2013).

29) T. Itani and T. Kozawa, Jpn. J. Appl. Phys. **52**, 010002 (2013).

30) J. J. Santillan, K. Yamada, and T. Itani, Appl. Phys. Express **7**, 016501 (2014).

31) J. Thackeray, T. H. Fedynyshyn, D. Kang, M. M. Rajaratnam, G. Wallraff, J. Opitz, and D. Hofer, J. Vac. Sci. Technol. B **14**, 4267 (1996).

32) M. T. Spuller, R. S. Perchuk, and D. W. Hess, J. Electrochem. Soc. **152**, G40 (2005).

33) C. Y. Hui and K. C. Wu, J. Appl. Phys. **61**, 5129 (1987).

34) Y. Tu and A. C. Ouano, IBM J. Res. Develop. **21**, 131 (1977).

35) N. L. Thomas and A. H. Windle, Polym. **23**, 529 (1982).

36) C. A. Mack, J. Electrochem. Soc.: Solid State Sci. Tehnol. **134**, 148 (1987).

37) C. Y. Hui, K. C. Wu, R. C. Lasky, and E. J. Kramer, J. Appl. Phys. **61**, 5137 (1987).

38) T. F. Yeh, H. Y. Shih, and A. Reiser, Macromolecules **25**, 5345 (1992).

39) T. Kudo, Y. Nanjo, Y. Nozaki, H. Yamaguchi, W. B. Kang, and G. Pawlowski, Jpn. J. Appl. Phys. **37**, 1010 (1998).

40) C. Decker, Polym. Int. **51**, 1141 (2002).

41) P. M. Johnson, J. W. Stansbury, and C. N. Bowman, Macromol. React. Eng. **3**, 522 (2009).

42) K. S. Anseth, C. M. Wang, and C. N. Bowman, Macromolecules **27**, 650 (1994).

43) M. Schmitt, RSC Adv. **4**, 1907 (2014).

44) M. Schmitt, Analyst **138**, 3758 (2013).

45) C. A. Bonino, J. E. Samorezov, O. Jeon, E. Alsberg, and S. A. Khan, Soft Matter **7**, 11510 (2011).

List of Publications

1. Comparison of radical generation efficiency of the oxime-based initiator radicals by galvinoxyl radical as an indicator

   Asuka Tsuneishi, Daisuke Sakamaki, Qi Gao, Takayuki Shoda, Takahiro Kozawa, and Shu Seki

   Japanese Journal of Applied Physics, in press

2. Dissolution behavior of negative-type photoresists for display manufacture studied by quartz crystal microbalance method

   Asuka Tsuneishi, Sachiyo Uchiyama, and Takahiro Kozawa

   Japanese Journal of Applied Physics 57, 46501, 2018

3. Relationship between C=C double bond conversion and dissolution kinetics in cross-linking-type photoresists for display manufacture, studied by real-time FTIR and quartz crystal microbalance methods

   Asuka Tsuneishi, Sachiyo Uchiyama, Ryouta Hayashi, Kentaro Taki, and Takahiro Kozawa

   Japanese Journal of Applied Physics, in press

Chapter 1

Comparison of radical generation efficiencies of the oxime-based initiator radicals using galvinoxyl radical as an indicator

1.1 Introduction

Photoradical initiators have been widely used in the photoprocessing of organic and polymeric materials,[1-9] and the quantum efficiency of free radicals via the initiators[10,11] upon exposure to light sources has been a key parameter to designing the platform of photopolymerization and/or photocrosslinking (curing) of polymers.[12] In this context, it is important to increase the absolute quantum efficiency of the initiators for pattern imaging at low exposure doses. Among the various types of initiators, oxime-type initiators[10-23] are a class of widely used initiators in the UV curing processing of resins. However, thus far, there have been only few reports on the systematic comparison of the efficiencies of such initiators, as well as on a comprehensive set of design rules to obtain a high efficiency in a series of oxime-type initiators. Herein, in this chapter, the author has introduced a facile method to determine experimentally the absolute quantum efficiency of the free radical generation of the initiators using a galvinoxyl radical (G) as a quencher. A small spectral overlap between the initiator and a quencher, as well as a stable spin on G, allows us a facile and precise determination of the radical yield via a marked electronic absorption and electron paramagnetic resonance (EPR) spectral change upon quenching. The theoretical calculation of the excited state of the initiator

well represents and predicts the overall change in the yield.

1.2 Experimental Procedure

Six kinds of oxime-type initiators (Received from Mitsubishi Chemical Corporation) were used, as shown in **Fig 1.1**. Photoirradiation was performed with a mercury lamp (Ushio USH-250D) equipped with a mask aligner (Mikasa M-1S) through an i-line bandpass filter. The photon fluence rate of the lamp was evaluated using a chemical actinometer with potassium ferrioxalate (III) and 1,10-phenanthroline in accordance with the literature.[24] Upon photoirradiation, sample solutions (3×10^{-3} dm^{-3}, 3 ml) were placed in a cylindrical cell (i.d. 4.2 cm) and irradiated from the top of the cell. The galvinoxyl radical was used as purchased (Tokyo Chemical Industry).

UV-Vis absorption spectra were obtained with a JASCO V–570 spectrometer. Absorption spectral change of PI-1 was measured in PI-1 toluene solution (0.5 mmol dm^{-3}) by irradiation of 365 nm-light. Absorption spectral change of the mixed solution of PI-1 and galvinoxyl radical was obtained in PI-1 and galvinoxyl toluene solution (0.1 mmol dm^{-3} each) by photo exposure at 365 nm.

EPR spectra at room temperature were recorded with a JEOL JES-FA-200 X-band spectrometer in PI-1 and galvinoxyl toluene solution (0.1 mmol dm^{-3} each) by photo exposure at 365 nm. Relative residues of galvinoxyl after photo exposure of 5.7×10^{-6} E (365 nm) monitored at the electronic transition of galvinoxyl at 433 nm against the relative concentrations of PI-1 to G galvinoxyl ([PI-1]/[G]) with PI-1 and galvinoxyl toluene solution (0.2 mmol dm^{-3} each).

The photodecomposition pattern of PI-1 was revealed, the solution with PI-1 and G

(0.1 mmol dm^{-3} each) after the exposure of 5.7×10^{-6} E was analyzed at room temperature by atmospheric pressure chemical ionization mass spectroscopy (APCI-MS). Low- and high-resolution atmospheric pressure chemical ionization mass spectra (APCI-MS) were obtained on a Thermo Fisher Exactive mass spectrometer at room temperature.

Relative residues of galvinoxyl after photo exposure monitored at the electronic transition of galvinoxyl at 433 nm of the mixed solutions of initiators and galvinoxyl ([[galvinoxyl] = 0.1 mmol dm^{-3}).

1.3 Results and Discussion

The protocols that lead to the absolute quantum efficiency of free radical initiators could be classified roughly into two categories upon UV photoexposure. The first category includes the protocols based on the amount (or the generation rate) of the resulting polymer[25] (or the consumption of the monomer) via the subsequent radical polymerization of monomers mixed with the initiators in the matrices by UV photoexposure. The second category includes the protocols focusing on the product analysis of the photodecomposed fragments of the initiators. In these cases, the amount of the initiator or the photogenerated (transient) species is traced quantitatively by spectroscopic[26] or chromatographic[27] analysis, enabling the indirect evaluation of the initial yields of free radicals given by the photodecomposition of the initiators. In this study, a direct radical scavenging protocol was applied to assess the initial yield, leading to the systematic comparison of the efficiencies of oxime-type initiators. The galvinoxyl radical (G), which is a commercially available π-conjugated organic radical with sufficiently high stability under the reaction condition of UV curing, was chosen as a

radical scavenger. The advantages of using G are 1) the characteristic narrow absorption peak at 433 nm with almost no overlap with the electronic absorption band of initiators, allowing us to precisely determine the residual/consumed concentration of G, 2) the transparent nature of G in the UV regime used in a typical curing process (around 350 nm), and 3) the expected miscibility of G with monomers with vinyl groups used in UV curing processes being higher than those of the other commercially available radical scavengers such as 2,2,6,6-tetramethylpiperidine 1-oxyl (TEMPO), presuming the competitive reactivity of G and monomers with photogenerated free radicals. Moreover, a series of 6 oxime-type initiators was investigated in this study as listed in **Fig. 1.1**

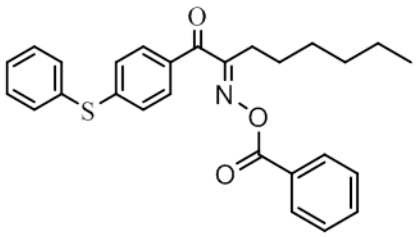

PI-1

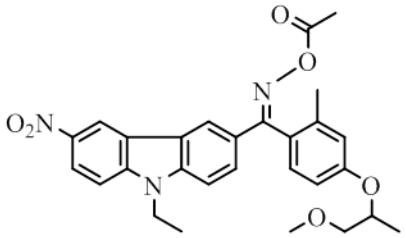

PI-2

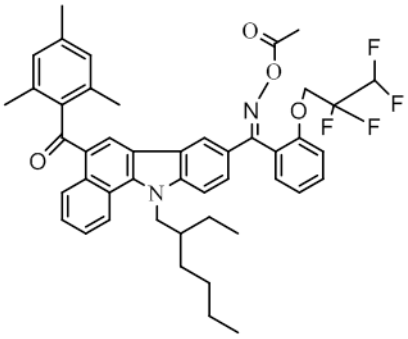

PI-3

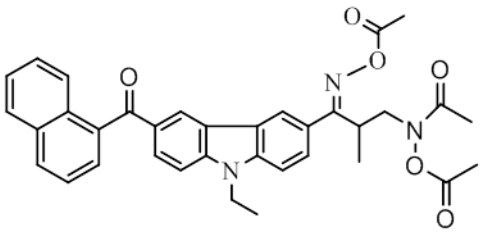

PI-4

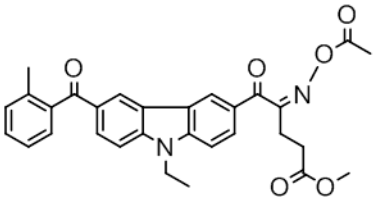

PI-5

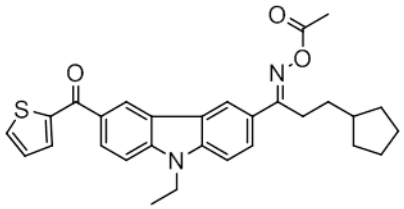

PI-6

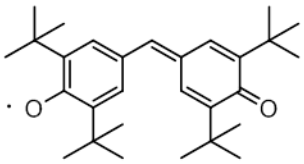

Galvinoxyl Radical (G)

Fig. 1.1. Chemical structures of the initiators and galvinoxyl radical.

The absolute quantum yield of free radicals was determined for the photochemical dissociation reaction of PI-1 in toluene by the sequential traces of near-UV electronic

absorption in accordance with the previous work.[26] Note that contributions from the other electronic transitions of the initiator were minimized using a bandpass filter to monochromate the i-line from the high-pressure Hg lamp employed. The initial electronic absorption of PI-1 at 330 nm decreased gradually upon exposure to 365 nm with the appearance of a new transition at around 300 nm as shown in Fig. 1.2. The spectral change is associated with two isosbestic points at 260 and 310 nm, and the initial characteristic peaks of PI-1 almost completely disappeared after 50 s photoexposure (irradiated photons = 1.4×10^{-5} E(einstein) cm^{-2}). The disappearance of the band at 330 nm and the appearance of the band at 300 nm suggest the photochemical dissociation of PI-1 resulting in the segmentation of the π-conjugated pathway and the shift to a higher energy region. The rate of the photochemical dissociation reaction of PI-1 (R_d) could be written as

$$R_d = \phi I_a = \phi l^{-1} I_0 (1 - 10^{-\varepsilon c l}) \qquad (1-1)$$

where ϕ is the quantum efficiency of the photochemical dissociation reaction of initiator PI-1, I_0 is the intensity of incident light (E $s^{-1}cm^{-2}$), I_a is the intensity of absorbed light ($cm^{-3}s^{-1}$), ε is the molar extinction coefficient of PI-1 at the wavelength of the irradiation light (365 nm), c is the concentration of PI-1, and l is the path length. The monitored optical density (absorbance) of PI-1 at 365 nm (A_t) is thus represented as

$$\ln(e^{2.303A_0} - 1) - \ln(e^{2.303A_t} - 1) = 2.303\phi I_0 \varepsilon t, \qquad (1-2)$$

where A_0 is the initial absorbance of PI-1 at 365 nm. I_0 was determined as 2.05×10^{-8} E s^{-1} cm^{-2} by chemical actinometry. The photodecomposition of PI-1 is well followed by Eq. (1－2) as represented in Fig. 3 with sufficiently high linearity. The slope of the linear correlation gives directly the absolute quantum efficiency of photodecomposition as $\phi = 0.46$.

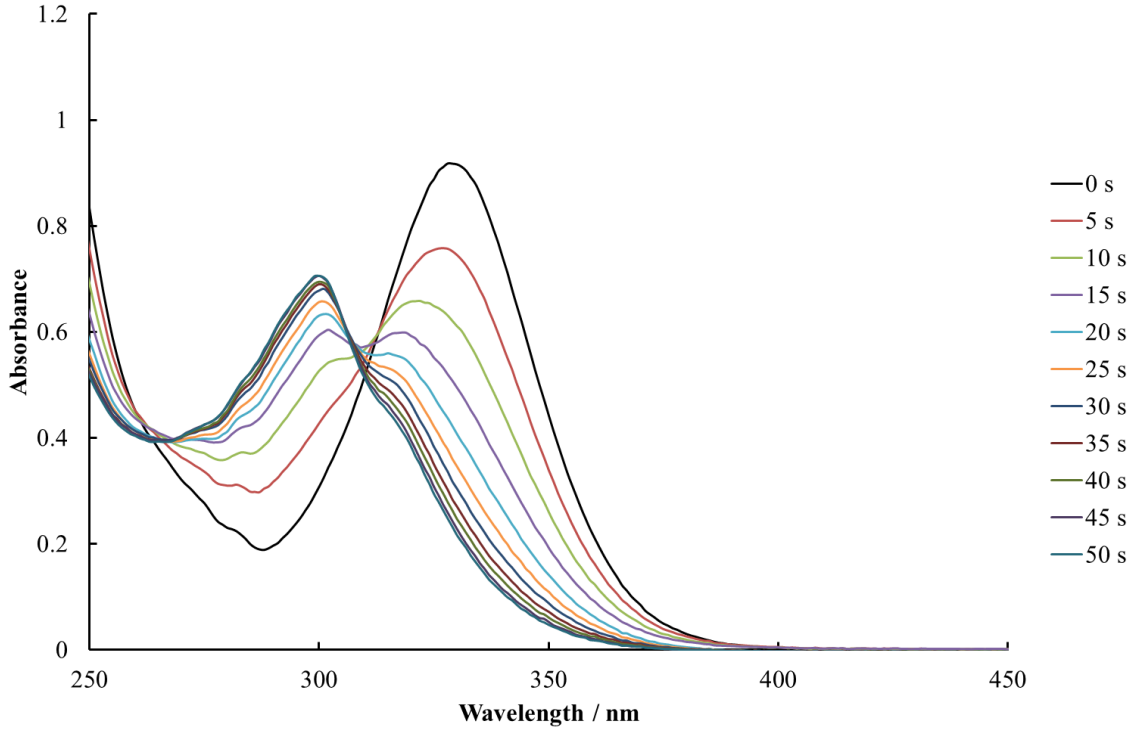

Fig. 1.2. Absorption spectral change of PI-1 in toluene solution (0.5 mmol dm^{-3}) by irradiation of 365 nm-light.

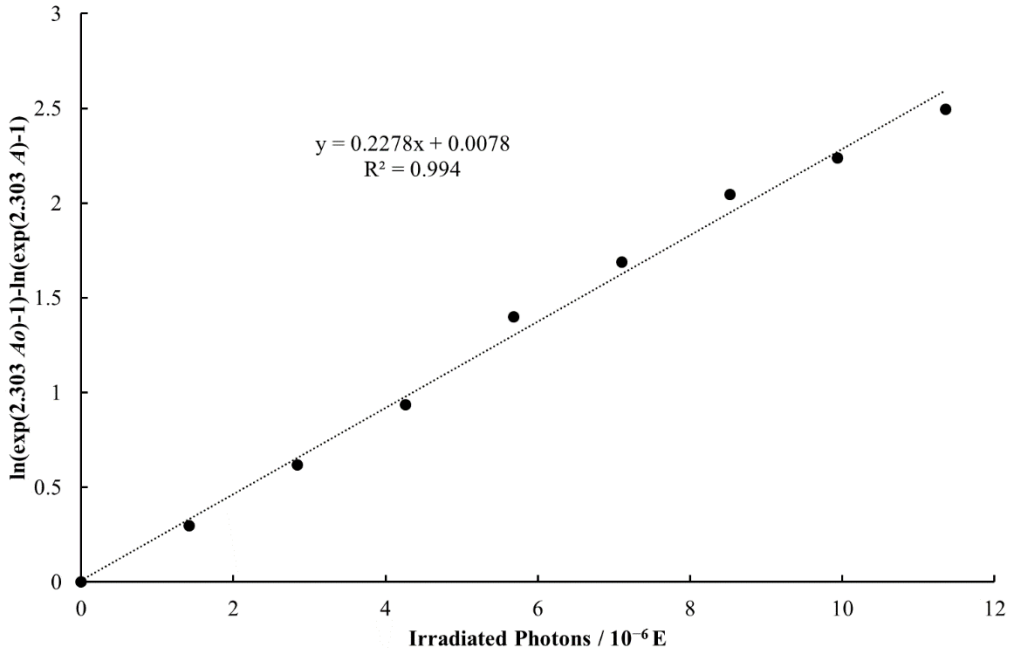

Fig. 1.3. Correlation between differential absorbance of PI-1 at 365 nm and irradiated photons.

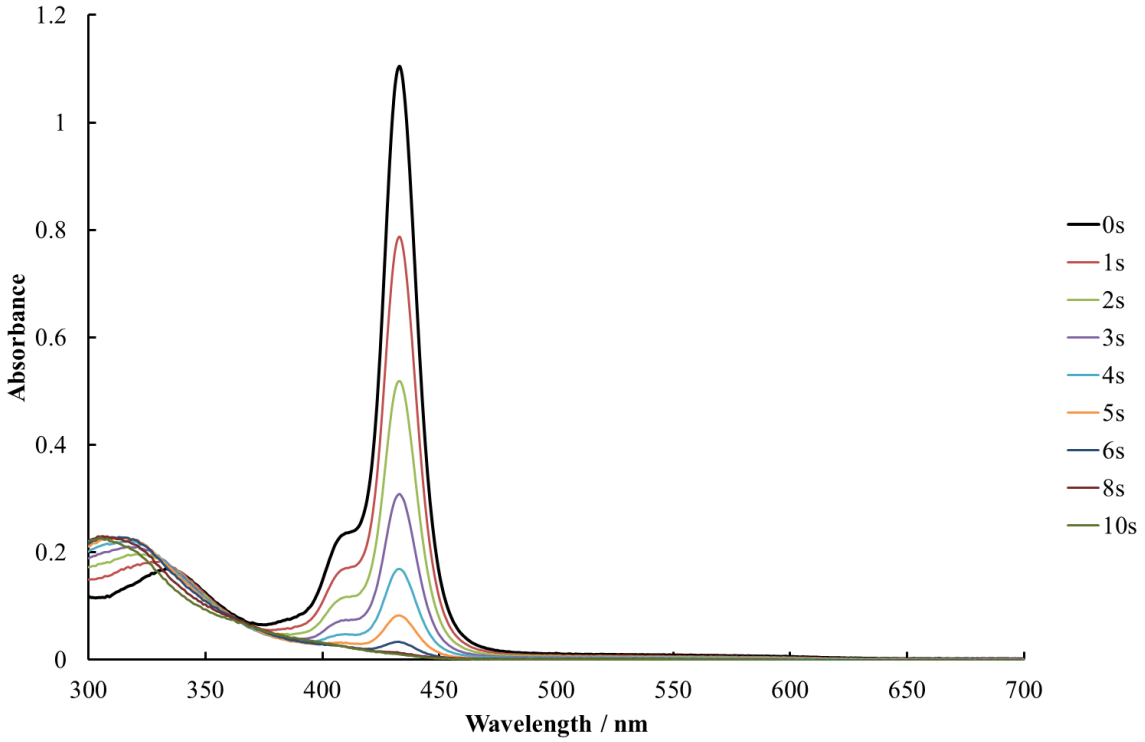

Fig. 1.4. Absorption spectral change of the mixed solution of PI-1 and G in toluene (0.1 mmol dm^{-3} each) by photo exposure at 365 nm.

Unfortunately, the analysis based on Eq. (1－2) is applicable only to the initiators with steady–state electronic transition at 365 nm. To assess all the other oxime-based initiators without the specific transition at the wavelength of the photoexposure source, direct quenching was conducted using G as a photogenerated free radical scavenger. Prior to the quenching scheme, the stability of G upon the photoexposure was confirmed, showing no change in the absorption spectral shape of G after 50 s photoexposure. Fig. 4 shows changes in the spectra of the equimolar toluene solution containing PI-1 and G (0.1 mmol dm^{-3} each). The characteristic sharp band of G decreases gradually upon photoexposure, suggesting the feasibility of G as an effective radical scavenger for the free radicals generated by the photodissociation of PI-1.

Note also that the high molar extinction coefficient of G at 433 nm ensured the sufficiently high sensitivity of G as an optical probe for the scavenging. After 10 s photoexposure (irradiated photons = 2.8×10^{-6} E), the optical density of G became negligible, and the EPR signal from the solution also showed the complete disappearance of G after 20 s photoexposure (**Fig. 1.5**). The total number of spins in photogenerated free radicals was estimated as the consumption of initial spins in G via radical recombination reactions with photogenerated ones. The solutions with a modulated relative concentration of PI-1 to G were exposed for a sufficient time (20 s), where the loaded PI-1 was photodecomposed completely, and the absorption spectra of the solutions were recorded. **Fig. 1.6** shows the change in the optical density of radicals monitored at 433 nm with respect to the molar ratio of PI-1 to G. The absorbance almost linearly decreased with increasing molar ratio of PI-1 and disappeared almost completely in cases with more than 0.5 equivalent of PI-1. This result suggests that one PI-1 molecule gives a pair of neutral radicals via a homolytic cleavage, quenched by two distinct Gs.

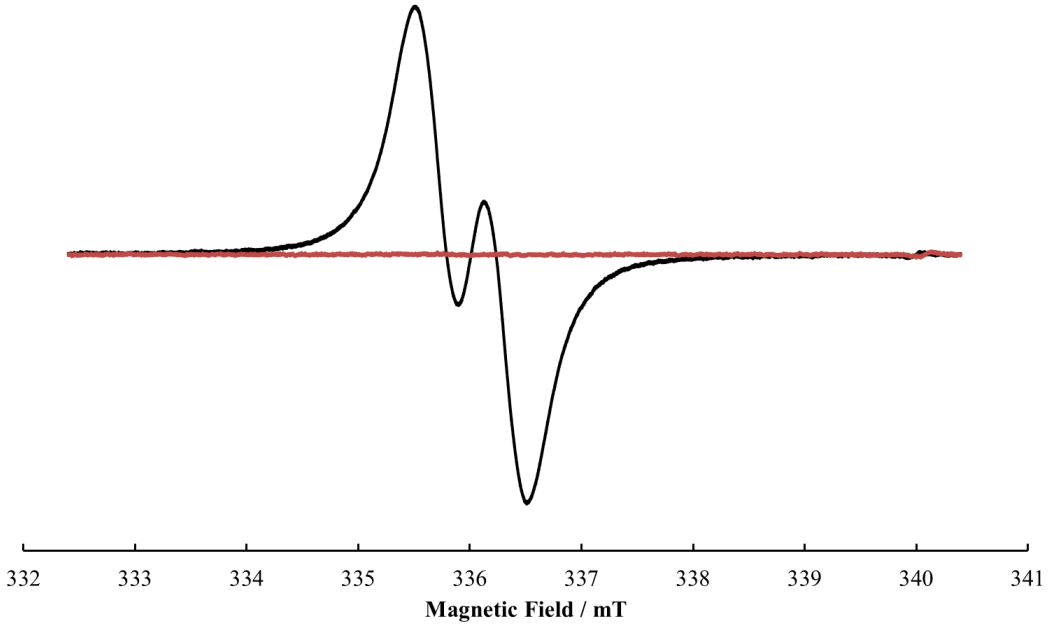

Fig. 1.5. EPR spectra of the mixed solution of PI-1 and G in toluene (0.1 mmol dm^{-3} each) before (black) and after (red) the exposure of 5.7 × 10^{-6} E (365 nm).

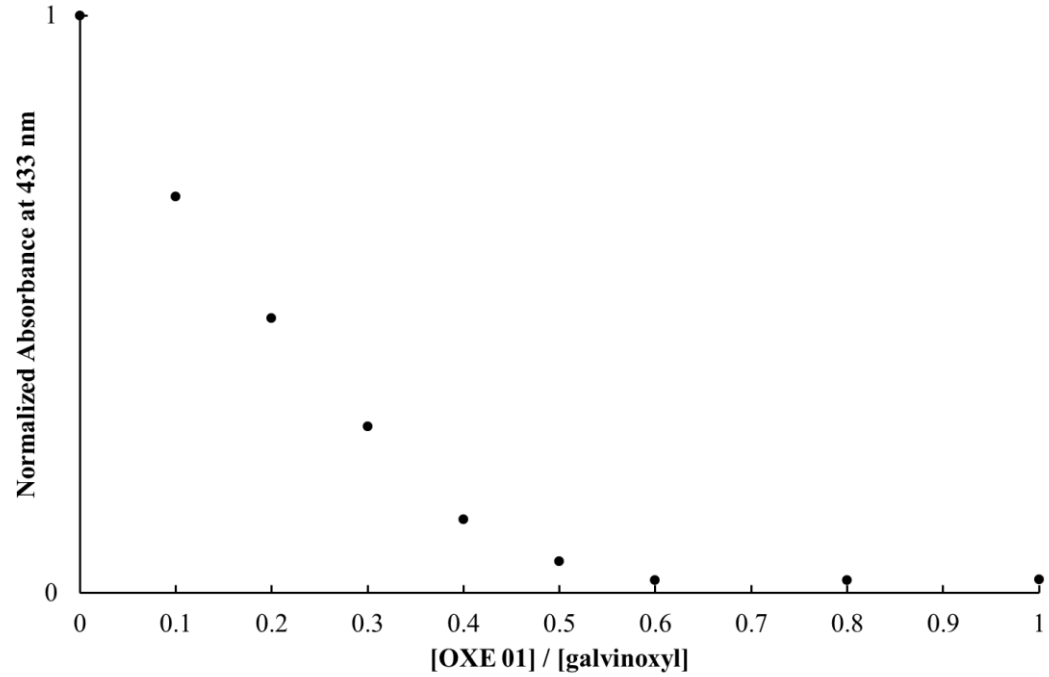

Fig. 1.6. Relative residues of G after photo exposure of 5.7 × 10^{-6} E (365 nm) monitored at the electronic transition of G at 433 nm against the relative concentrations of PI-1 to G ([PI-1] / [G]).

To clarify the photodecomposition pattern of PI-1, the solution with PI-1 and G (0.1 mmol dm^{-3} each) after the exposure of 5.7×10^{-6} E was analyzed by atmospheric pressure chemical ionization mass spectroscopy (APCI-MS). The observed mass spectrum is shown in **Fig. 1.7** with an approximately 750 Da magnified view, indicating unequivocally the formation of 1 represented as the superimposed one (or its structural isomer), which corresponds to the product of the radical coupling reaction between G and a fragment of PI-1.

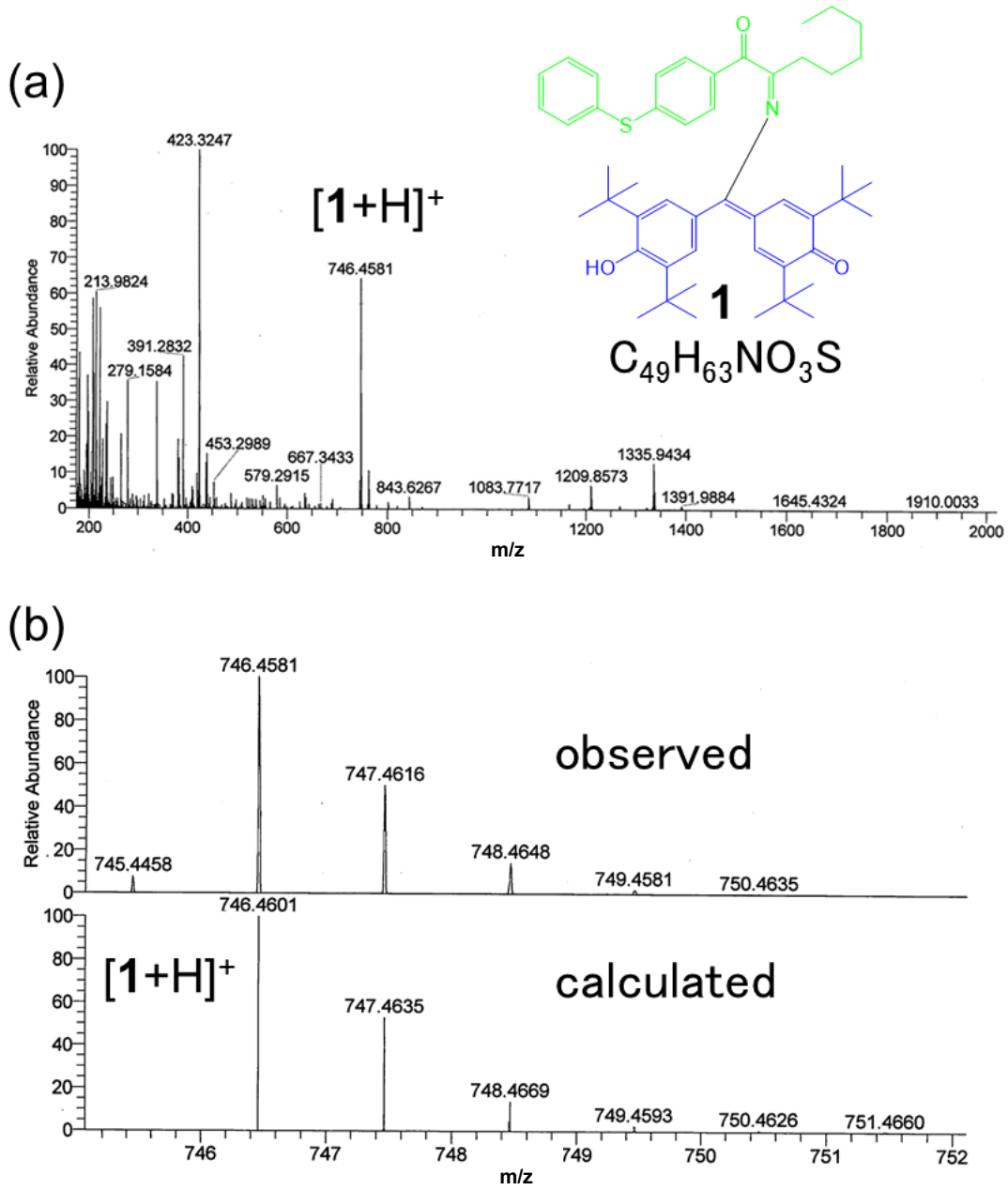

Fig. 1.7. (a) APCI high-resolution mass spectra of the resulting solution of the reaction of PI-1 and G. (b) Magnified view of the peaks (around 746 Da).

The quenching experiment in an identical protocol with G was performed for the other five different initiators, and the photodecomposition of the initiators are monitored as summarized in **Fig.1. 8**.

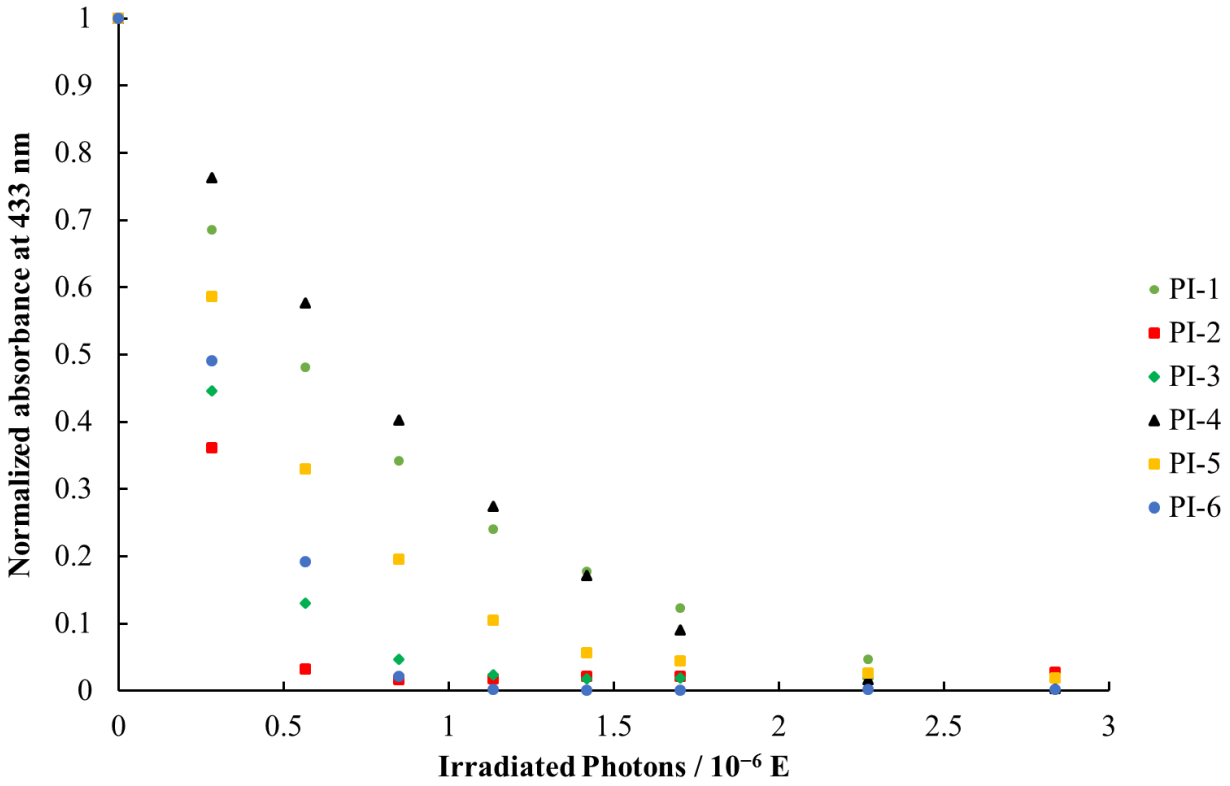

Fig. 1.8. Relative residues of G after photo exposure monitored at the electronic transition of G at 433 nm of the mixed solutions of initiators and G ([PI] = [G] = 0.1 mmol dm^{-3}).

Herein, as a measure of the relative photodecomposition reaction efficiency of the initiators giving effective free radicals for the subsequent radical initiated reactions, an effective quenching efficiency is defined as

$$\phi_{\text{eff}} = \frac{cV(1 - A_{\text{norm,1 sec}})}{I_0 S}, \qquad (1-3)$$

where c, V, $A_{\text{norm,1 s}}$, and S are the concentration of the initiator, the volume of the solution, the normalized absorbance of G at 433 nm after 1 s irradiation, and the photoexposure spot area, respectively. ϕ_{eff} corresponds to the number of G consumed

per photons. The calculated ϕ_{eff} values for the series of initiators are summarized in Table I. Note that the ϕ_{eff} (0.33) of PI-1 was different from the ϕ (0.46) of PI-1. ϕ is defined as the number of photodecomposed initiator molecules per absorbed photon; ϕ_{eff} is the number of quenched galvinoxyl radicals per incident photon. The former is expected to be identical to or higher than the latter, which reflects well the yield of radicals contributing to the subsequent reactions.

1.3.2 Theoretical aspects on quantum efficiency of photo-radical initiators

ϕ_{eff} values were also obtained by quantum chemical calculations. The structures of the six initiators were optimized at the singlet ground state using the hybrid B3LYP Hamiltonian with the 6-31G(d,p) basis set. Using the optimized structures, the 20 lowest excitation energies (v_i) as well as the oscillator strength (f_i) of these initiators were calculated by a time-dependent density functional theory (TD DFT) method. All the quantum calculations were performed with the Gaussian 09 program. The absorption spectra $\mathrm{A}(v)$ of these initiators were simulated via a Gaussian broadening protocol represented as

$$\mathrm{A}(v) = 2.174 \times 10^8 \sum_{i=1}^{20} \frac{f_i}{\sigma} \exp\left(-2.773 \frac{(v - v_i)^2}{\sigma^2}\right) \qquad (1-4)$$

The line width (σ) of the Gaussian functions was set at 3000 cm^{-1} with reference to the corresponding experimental spectra. The light absorptivity of each initiator (f_{abs}) was given by the numerical integration of the simulated spectral segment (**Fig. 1.9**) overlapped with the spectrum of the exposure light source (**Fig. 1.10**).

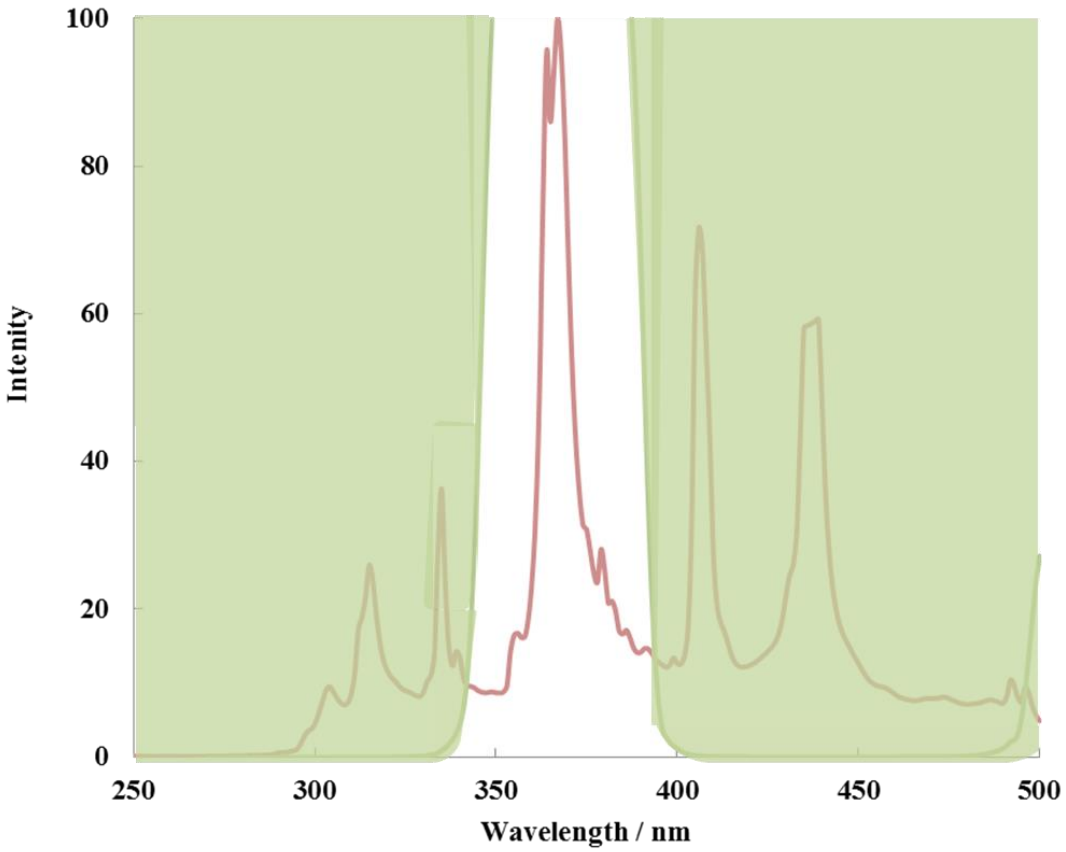

Fig. 1.9. The spectrum of an excitation light source overlapped with the transmittance profile of the bandpass filter used in the present study.

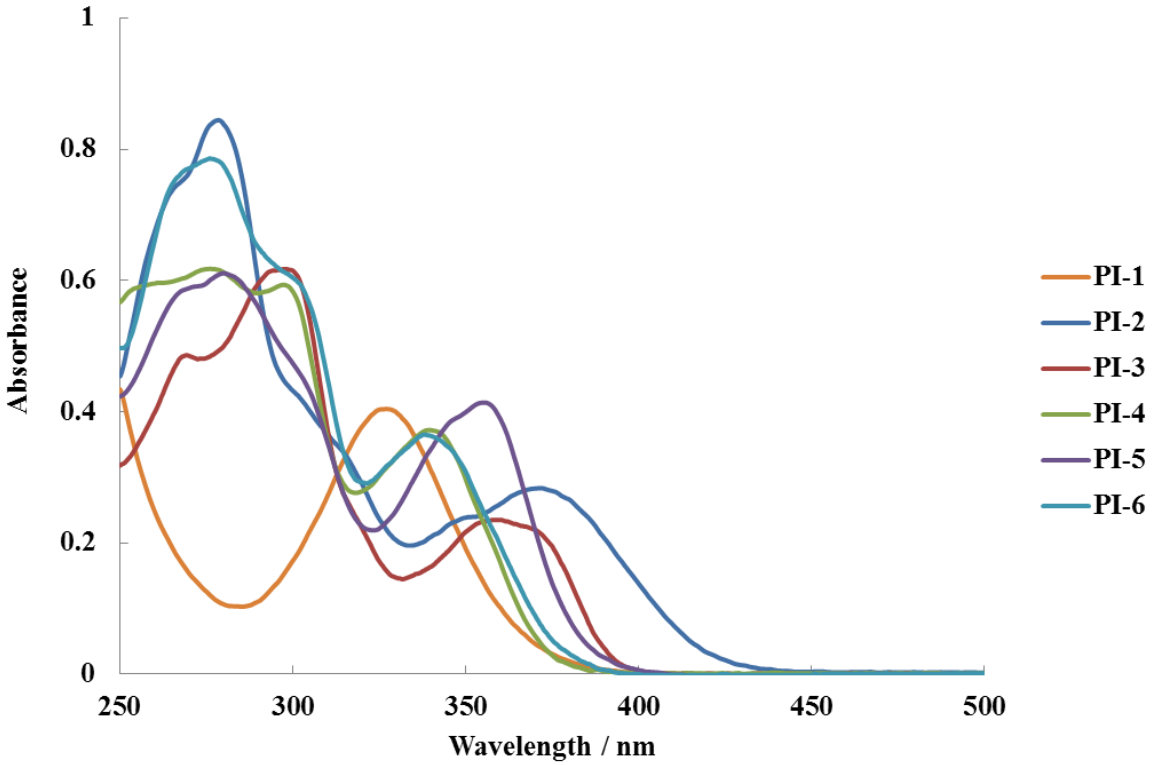

Fig. 1.10. The absorption spectra of PI-1-6.

A factor proportional to the intersystem crossing efficiency of the initiators (f_{ISC}) was calculated as[28)]

$$f_{ISC} = \frac{< \mathrm{T_1}|H_{\mathrm{SO}}|\mathrm{S_1} >^2}{(\Delta E_{\mathrm{S1-T1}})^2} \qquad (1-5)$$

where H_{SO} and $\Delta E_{\mathrm{S1-T1}}$ are the spin-orbit operator and the energy difference between the S_1 and T_1 states, respectively. The structure for calculating the property was the optimized structure at the first excited singlet state, which was calculated using the hybrid B3LYP method with 6-31G(d,p) basis sets. The structure optimization was performed with the Gaussian09 program and the f_{ISC} calculation was performed with

the Dalton program.

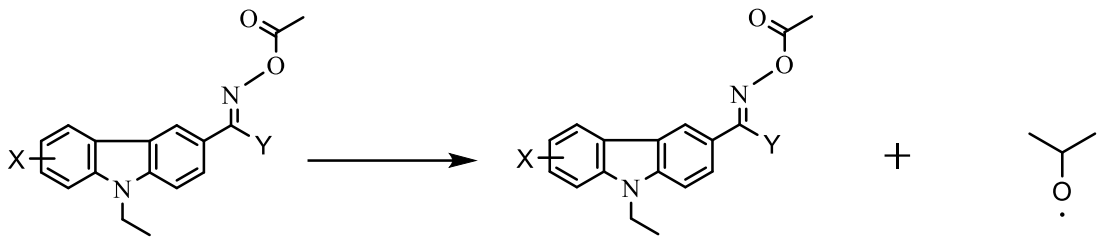

Fig. 1.11. Presumed photodecomposition reaction.

By presuming the photodecomposition reaction represented in Fig. 1.11, the efficiency of the dissociation reactions at the N–O bond in the initiators at the T_1 level (f_{diss}) was defined as[29)]

$$f_{\mathrm{diss}} = \exp\left(-\frac{k_{\mathrm{B}}T}{\Delta H_{\mathrm{diss}}}\right) \qquad (1-6)$$

Since all of the initiators employed in the present study take a homogeneous structure around the photodecomposition point of N–O, it is acceptable to presume the following hypothesis: f_{diss} satisfactorily correlates with ΔH_{diss}. Here, ΔH_{diss} is referred to as the enthalpy of the bond dissociation reactions occurring at the T_1 state. ΔH_{diss} was determined as the difference between the energy of the dissociation reaction and the energy of the initiator at the T_1 state. The energy for transient/radical species was obtained by using the hybrid UB3LYP Hamiltonians with 6-31G (d,p) basis sets. All these calculations were carried out with the Gaussian 09 program. Consequently, the parameter reflecting the radical generation efficiency (f_{rg}) was given as

$$f_{rg} = f_{abs} \times f_{ISC} \times f_{diss} \quad (1—7)$$

and the derived f_{rg} values are summarized in **Table I** together with the f_{abs}, f_{ISC}, and f_{diss} values. Our calculation results show good correlation with the ϕ_{eff} values determined by the above experimental protocols (**Fig**. **1.12**). Note that f_{ISC} is underestimated particularly for PI-1 and PI-6 owing to the insufficient heavy atom effects taken into account for spin-orbit coupling on sulfur atoms in the compounds. This is the case for the lower f_{rg} relative to the experimentally determined ϕ_{eff} as seen in **Table 1.1** (and in **Fig**. **1.12**).

Table 1.1. Effective quantum efficiency ϕ_{eff} and theoretically predicted f values.

Photoinitiator	ϕ_{eff}	f_{abs}	f_{ISC}	f_{diss}	f_{rg}
PI-1	0.33	0.23	0.56	0.93	0.12
PI-2	0.68	1	5.97	0.88	5.29
PI-3	0.59	0.75	6.96	0.91	4.72
PI-4	0.25	0.34	4.18	0.87	1.22
PI-5	0.44	0.91	3.69	0.93	3.12
PI-6	0.54	0.43	7.05	0.93	2.83

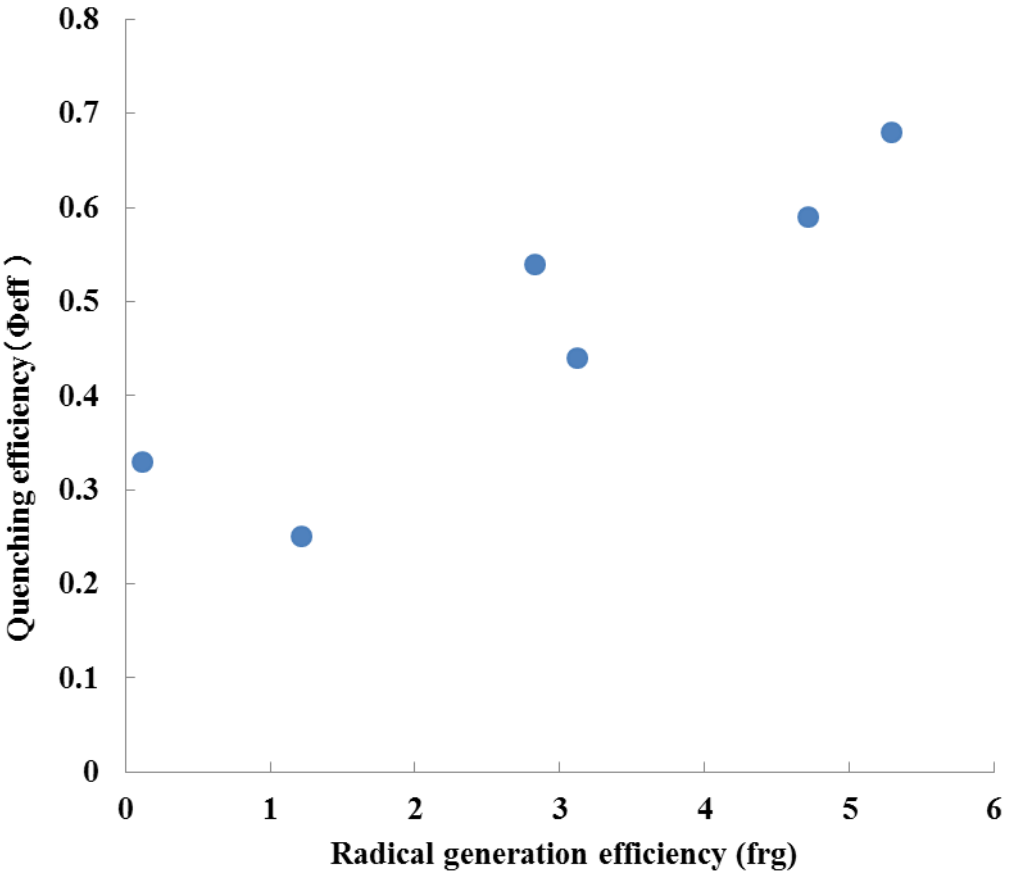

Fig. 1.12. Comparison between the quenching efficiency by experiment and radical generation efficiency by theoretical calculation.

Among all the initiators examined, PI-6 showed high f_{ISC} values in theoretical protocols. To rationalize the intersystem crossing (ISC) processes of the initiators, the transient excited states of the initiators were investigated in terms of the spatial distribution/symmetry of molecular orbitals.

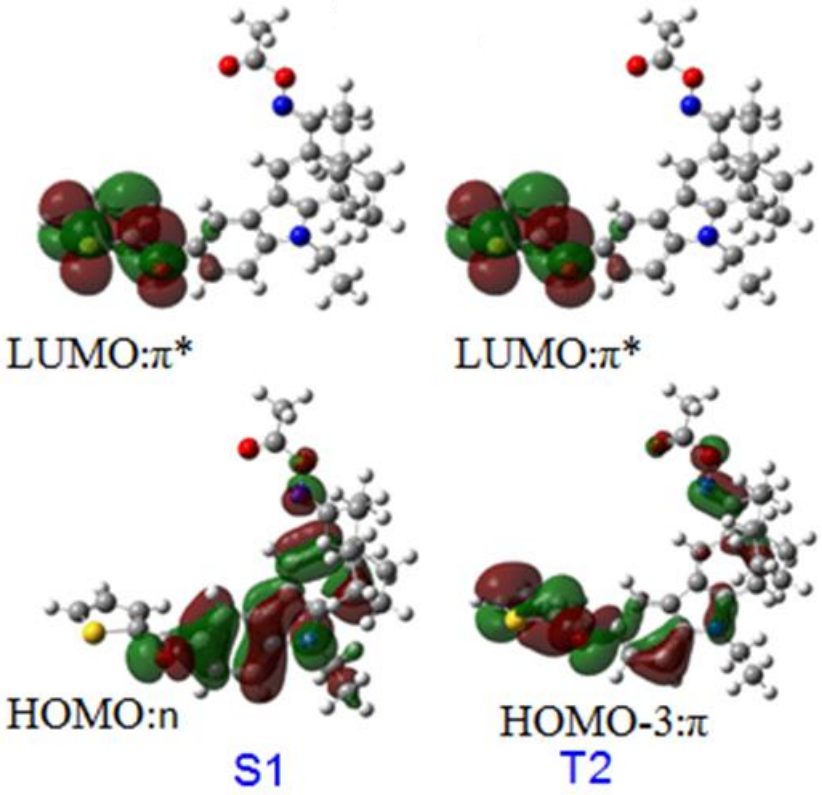

Fig. 1.13. Frontier orbital representation of S_1 and T_2 states of PI-6.

Fig. 1.13 shows the frontier MOs of PI-6 at the S_1 and T_2 states. The S_1 state of PI-6 is predominantly produced via the transition from the n orbital on the carbonyl group bound to the π* orbital on the carbazole group, referred to as the nπ* transition. From the systematic survey of the orbital symmetry of the triplet excited states of PI-6 contributing mainly to the subsequent photodecomposition reactions of PI-6, I found the T_2 state of PI-6, giving a good representative orbital overlap with the S_1 state with small discrepancy in those energy levels (**Fig. 1.13**). According to the El-Sayed rule, the intersystem crossing between S_1 (nπ*) and T_2 (ππ*) is allowed, and this is the case

leading to the efficient intersystem crossing in PI-6. In contrast, PI-1 has diphenyl sulfide in its main π-conjugated core without the carbonyl group directly attached to the core. The small contribution of nπ* to the S_1 state in PI-6 causes a considerable reduction in overlap onto the $T_1(\pi\pi^*)$ state, lowering the efficiency of intersystem crossing. This suggests that the S_1 state with nπ* nature plays a key role in the design of initiator molecules interplaying the high light absorptivity and the resulting high quantum yield via intersystem crossing triplet states.

1.4 Conclusions

In summary, the author has investigated a facile method to evaluate the free radical yield using G as a radical quencher, which reacts efficiently with the photogenerated radicals from a series of initiators upon near-UV photoexposure. The experimentally determined quantum efficiencies are well reproduced by those from full theoretical calculations. The key role of S_1 state symmetry overlapping with that of T_2 state has been revealed for initiators with efficient intersystem crossing and high overall quantum efficiency of free radical formation, suggesting the validity of the full theoretical approach by quantum chemical calculation to predict quantitatively the quantum efficiency, and for the future design of high-performance initiators.

References

1) R. W. Sabnis, Displays **20**, 119 (1999).

2) H. F. Gruber, Prog. Polym. Sci. **17**, 953 (1992).

3) J. Eichler and P. Herz, J. Photochem. **12**, 225 (1980).

4) C. Decker, Polym. Int. **51**, 1141 (2002).

5) S. Jockusch, I. V. Koptyug, P. F. McGarry, G. W. Sluggett, N. J. Turro, and D. M. Watkins, J. AM. Chem. Soc. **119**, 11495 (1997).

6) T. Sumiyoshi, W. Schnabel, A. Henne, and P. Lechtken, Polym. **26**, 141 (1985).

7) J. Choi, W. Lee, J. W. Namgoong, T.-M. Kim, and J. P. Kim, Dyes Pigm. **99**, 357 (2013).

8) K. Tsuda, Displays, **14**, 115 (1993).

9) W. G. Kim and J. Y. Lee, Polym. **44**, 6303 (2003).

10) D. Shiota, Y. Tadokoro, K. Noda, M. Shiba, and M. Fujii, J. Photopolym. Sci. Technol. **24**, 625 (2011).

11) Y. Muramatsu, M. Kaji, A. Unno, and O. Hirai, J. Photopolym. Sci. Technol. **23**, 447 (2010).

12) D. E. Fast, A. Lauer, J. P. Menzel, A.-M. Kelterer, G. Gescheidt, and C.

Barner-Kowollik Macromolecules **50**, 1815 (2017).

13) C. J. Groenenboom, H. J. Hageman, P. Oosterhoff, T. Overeem, and J. Verbeek, J. Photochem. Photobiol. A **107**, 261 (1997).

14) F. Amat-Guerri, R. Mallavia, and R. Sastre, J. Photopolym. Sci. Technol. **8**, 205 (1995).

15) M. Yoshida, H. Sakuragi, T. Nishimura, S. Ishikawa, and K. Tokumaru, Chem. Lett. 1125 (1975).

16) P. Baas and H. Cerfontain, J. Chem. Soc. Perkin II 156 (1979).

17) P. Baas and H. Cerfontain, J. Chem. Soc. Perkin II 1653 (1979).

18) R. Mallavia, R. Sastre, and F. Amat-Guerri, J. Photochem. Photobiol. A. **138**, 193 (2001).193 (2001).

19) Y. Miyake, H. Takahashi, N. Akai, K. Shibuya, and A. Kawai, Chem. Lett. **43**, 1275 (2014).

20) X. Allonas, J. Lalevée, J. –P. Fouassier, H. Tachi, M. Shirai, and M.Tsunooka, Chem. Lett. 1090 (2000).

21) G. A. Delzenne, U. Laridon, and H. Peeters, Euro. Polym. J. **6**, 933 (1970).

22) C. Dietlin, J. Lalevee, X. Allonas, J. P. Fouassier, M. Visconti, G. Li Bassi, and G. Norcin, J. App. Polym. Sci. **107**, 246 (2008).

23) J. V. Crivello and E. Reichmanis, Chem. Mater. **26**, 533 (2014).

24) A. Fujishima, R. Baba, and K. Kawano, Chemical Education, **440**, 35 (1987) [in Japanese].

25) J. C. Bevington, J. H. Bradbury, and G. M. Burnett, J. Polym. Sci. **12**, 469 (1954).

26) P. Smith and A. M. Rosenberg, J. Am. Chem. Soc. **81**, 2037 (1959).

27) C. J. Groenenboom, H. J. Hageman, T. Overeem, and A. J. M. Weber, Macromol. Chem. **183**, 281 (1982).

28) Y. L. Chen, S. W. Li, Y. Chi, Y. M. Cheng, S. C. Pu, Y. S. Yeh, and P. T. Chou, ChemPhysChem **6**, 2012 (2005).

29) J. Lalevée, N. Blanchard, M. El-Roz, X. Allonas, and J. P. Fouassier, Macromolecules **41**, 2347 (2008).

Chapter 2

Dissolution behavior of negative-type photoresists for display manufacturing, studied by quartz crystal microbalance method

2.1 Introduction

The dissolution processes have been widely investigated because they have a significant impact on the formation of resist surface profiles. The dissolution processes have been investigated by visible and infrared reflectance spectroscopy,[6-8] quartz crystal microbalance (QCM),[8-13] high speed atomic force microscopy (AFM),[14-18] Rutherford backscattering spectrometry,[19] simulation,[20-24] and other methods.[25,26] The dissolution kinetics and their dependence on exposure dose (reaction rate),[6,9] molecular structures,[8,11] film thickness,[15] acidity,[8,11,26] and pattern shape[16] have been widely studied. In particular, the transient swelling has been intensively studied.[7,8,10-12,15,16,19] However, these studies were mainly focused on the positive-type resist materials for manufacturing semiconductor devices. The studies on the dissolution kinetics of resist materials for manufacturing displays were few.[25] It is known that the shape of resist after development varies depending on the polymer type, even in the same photo-curing system of negative-type photoresists. It has been reported that the dissolution behavior of the polymer is affected by the acid value of the polymers. The acid value is expressed in mg of potassium hydroxide (KOH) required to neutralize the acidic component contained in 1 g of a polymer. When the acid value was high, the dissolution rate became

fast and the development type also became homogeneous dissolution.[25] However, the details in the dissolution behavior of negative-type photoresists for display manufacturing are still unknown.

In this chapter, the author analyzed the development processes in a TMAH aqueous solution to clarify the basic dissolution mechanisms of the negative-type photoresists used for the display manufacturing. The dissolution kinetics of six kinds of polymers was measured in the absence and presence of the low-molecular-weight components (a monomer, a photoinitiator, and a surfactant) with a QCM method. The mixing ratio of polymer and monomer was also changed. The dependence of dissolution kinetics on the molecular structure of polymers and the effects of low-molecular-weight components are discussed. Understanding of the dissolution behavior is essential for the efficient development of resist materials and the accurate simulation of resist pattern formation.

2.2 Experimental Procedure

Six kinds of polymers (Received from Mitsubishi Chemical Corporation) were used, as shown in **Fig 2.1**. The molecular weights and acid values of the polymers are listed in **Table 2.1**. The samples with and without the monomer components are hereafter called polymer and resist samples (or films), respectively. For the polymer samples, the polymers shown in **Fig. 2.1** were dissolved in propyleneglycol monomethyl ether acetate (PGMEA) before the spin-coating. The resist samples consisted of a polymer (Polymer-C, D, and E), a monomer, a photoinitiator and a surfactant. The resist samples with Polymer-C, D, and E are hereafter called Resist-C, D, and E, respectively. Di-pentaerythritol polyacrylate was used as a monomer. 1-[4-(phenylthio)phenyl]-1,2-octanedione 2-(o-benzoyloxime) (Purchased BASF) was

used as a photoinitiator. The concentration of photoinitiator was 2 wt% to the sum of polymer and monomer weights. A fluorochemical surfactant(Received from Mitsubishi Chemical Corporation) was used. The concentration of surfactant was 0.1 wt%. The surfactant was used for the uniform film forming. It was confirmed that the 0.1 wt% surfactant did not affect the dissolution kinetics. The weight ratio between the polymer and the monomer in each resist sample was changed from 75:25 to 50:50 and 25:75. The resist samples were also dissolved in PGMEA before spin-coating.

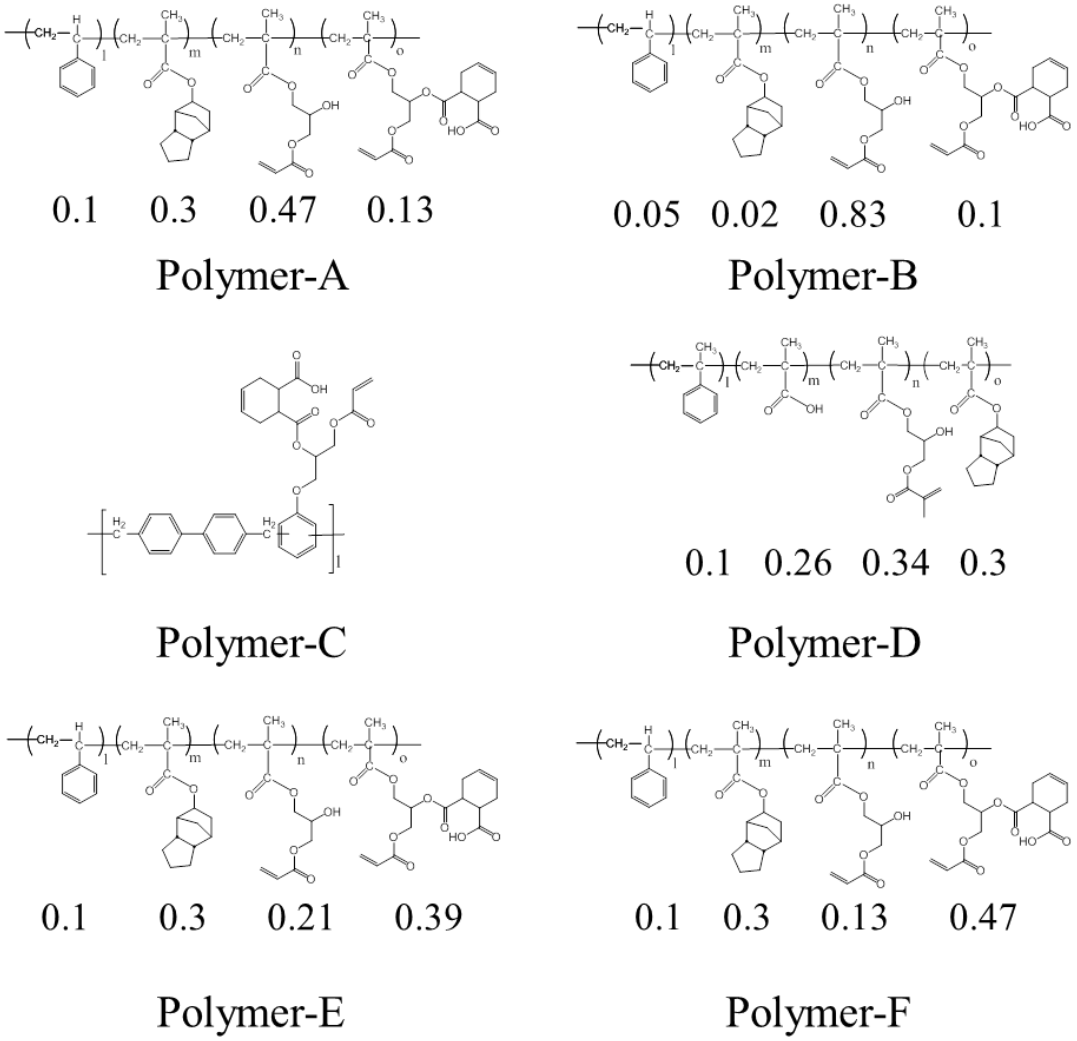

Fig. 2.1. Molecular structures of polymers. The numerical values below the molecular structures denote the molar ratio of monomer units.

Table 2.1. Molecular weights (Mw) and acid values of polymers.

Sample	Mw	Acid value (mg KOH/g)
Polymer-A	8200	30
Polymer-B	9000	30
Polymer-C	6000	60
Polymer-D	7400	78
Polymer-E	8400	80
Polymer-F	5300	91

The polymer sample solutions were spin-coated on the QCM substrates and baked at 90 °C for 120s s to form the polymer films with the thicknesses of 50, 100, 500, and 800 nm. The resist sample solutions were also spin-coated on the QCM substrates and baked at 90 °C for 120 s to form the resist film with the thickness of 500 nm.

The dissolution kinetics of polymer and resist samples were measured by the QCM-based development analyzer (Litho Tech Japan RDA-Qz^3).[10] 2.38% TMAH aqueous solution (Tokyo Ohka Kogyo NMD-3) was used as an aqueous base developer. For a thin, rigid film applied to the crystal surface, the frequency shift ΔF is linear with the mass of the applied film:[8,27]

$$\Delta F = -\frac{2F_0^2}{\sqrt{\rho_Q \mu_Q}} m' \qquad (2-1)$$

Here, F_0 is the resonant frequency at the unloaded QCM substrate, m' is the mass of the film, ρ_Q is the density of the quartz crystal, and μ_Q is its shear modulus corrected for

piezoelectric stiffening. The measurement of each sample was performed up to eight times. A representative dissolution kinetics for each sample was shown. The measurement values such as dissolution time were averaged and listed in tables. The dissolution time was defined as the time when the apparent mass of the film (including the impregnated developer) was decreased to half of the original mass before development.

2.3 Results and Discussion

2.3.1 The dissolution behaviors of only polymer

Fig. 2.2 shows the representative measurement results for the frequency changes of QCM substrates with Polymer-A. The acid value of Polymer-A was 30 mg KOH/g. The initial thicknesses of polymer films were 50, 100, 500, and 800 nm. Upon the insertion of QCM substrates into the developer, the frequency immediately dropped by approximately 660 Hz due to the increase in the viscosity of their surroundings.

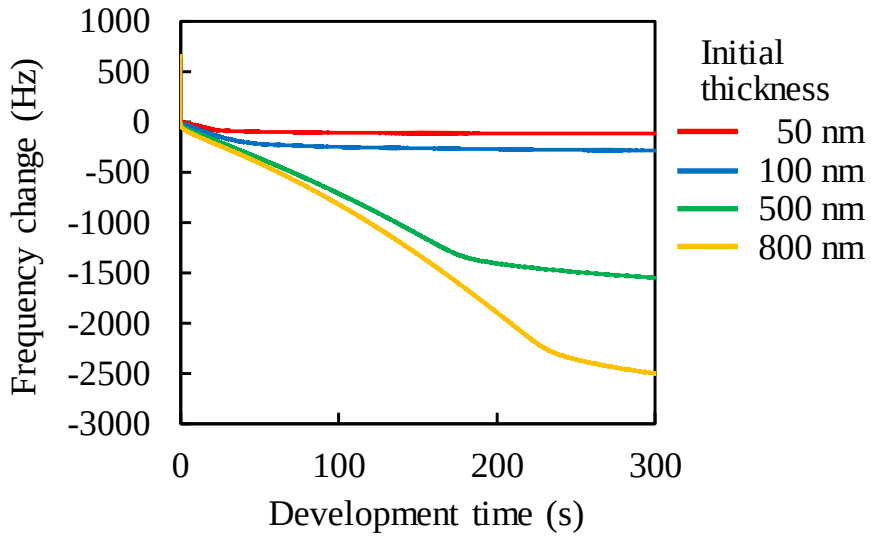

Fig. 2.2. Representative measurement results for the frequency changes of QCM substrates with Polymer-A during development.

Table 2.2. Average dissolution time and frequency reduction for Polymer-A.

Sample	Film thickness (nm)	Dissolution time (s)	Frequency reduction (Hz)
Polymer-A	50	Not dissolved	138.7
	100	Not dissolved	318.1
	500	Not dissolved	1710.4
	800	Not dissolved	2808.5

The frequency immediately after the drop was set to be 0 (a base) and the frequency change was plotted in the graph. After the initial drop, the frequency gradually decreased. The decrease rates of frequencies for the thicknesses of 50, 100, 500, and 800 nm were largely changed approximately at the development time t_{dev} = 20, 30, 170, and 220 s, respectively (inflection points). This suggests that the developer reached the interface between polymer film and QCM substrate at the inflection points. The frequencies at the inflection points were -76.2, -172.8, -1285.4, and -2141.9 Hz for the thicknesses of 50, 100, 500, and 800 nm, respectively. The decrease in the frequency is due to the increase of the mass of polymer films, as indicated by Eq. (1). The increase of mass was caused by the penetration of developer into the resist film. For all thicknesses, the decrease rates in the frequency were accelerated with the development time until the inflection points. The acceleration is considered to be caused by the softening of the polymer film owing to the developer impregnation. After the development, the thickness of polymer films was measured. It was found that the film thickness was not significantly changed before and after the development. All the polymers used in this

study are soluble in the TMAH aqueous solution when they are used as a matrix polymer of the negative-type resist. It has been reported that the critical entanglement molecular weights of poly(methyl methacrylate) (PMMA) and polystyrene (PS) were 18400 and 31200, respectively.[28] The corresponding number of monomer units for PMMA and PS are 184 and 300, respectively. The numbers of monomer units of the polymers used in this study are well below such values. Therefore, it can be assumed that the effects of polymer entanglement on developer penetration and polymer dissolution are weak for all the polymers used in this study. This fact does not contradict with the rapid intake of developer. Nevertheless, Polymer-A was insoluble in the absence of the other resist components. The insoluble property of Polymer-A is considered to be owing to the hydrophobic interaction.[29,30] The absolute value of the lowest frequency change during the development was defined as "frequency reduction", which is hereafter used as an indicator of the swelling of films caused by the developer penetration. The average dissolution time and frequency reduction for Polymer-A are summarized in **Table 2.2**. The dissolution times were "Not dissolved" for all the samples. The frequency reductions at t_{dev} = 300 s were listed. The frequency reduction was roughly proportional to the initial film thickness. This result also suggests that the developer reached the interface between polymer film and QCM substrate.

The molar ratio of hydrophobic groups of Polymer-A was decreased to examine the effect of hydrophobic interaction. The representative measurement results of Polymer-B are shown in **Fig. 2.3(a).** Except for the polymer film with the initial film thickness of 50 nm, the polymer films were dissolved. For the initial thickness of 800 nm, the frequency was decreased and slightly increased with the progress of development. After that, the frequency abruptly rose and started to vibrate severely at t_{dev} = 1.348 s. Note that the

frequency vibration was omitted from the graph for the clear display. The vibration suggested that the dissolution of these polymer films is not smooth. The polymer layer was considered to be peeled off by shear as microscopic flake.[25,26] Hereafter, such development is called a peeling type development. For the initial thickness of 500 nm, a similar behavior was observed. The onset of peeling was delayed, compared with the case of the initial thickness of 800 nm.

The effects of acid values were investigated by increasing the acid values. **Fig. 2.3(b)** shows the representative measurement results for the frequency changes of QCM substrates with Polymer-C with the acid value of 60 mg KOH/g. The polymer films with the initial thicknesses of 50 and 100 nm were not still dissolved although the frequency reduction was increased.

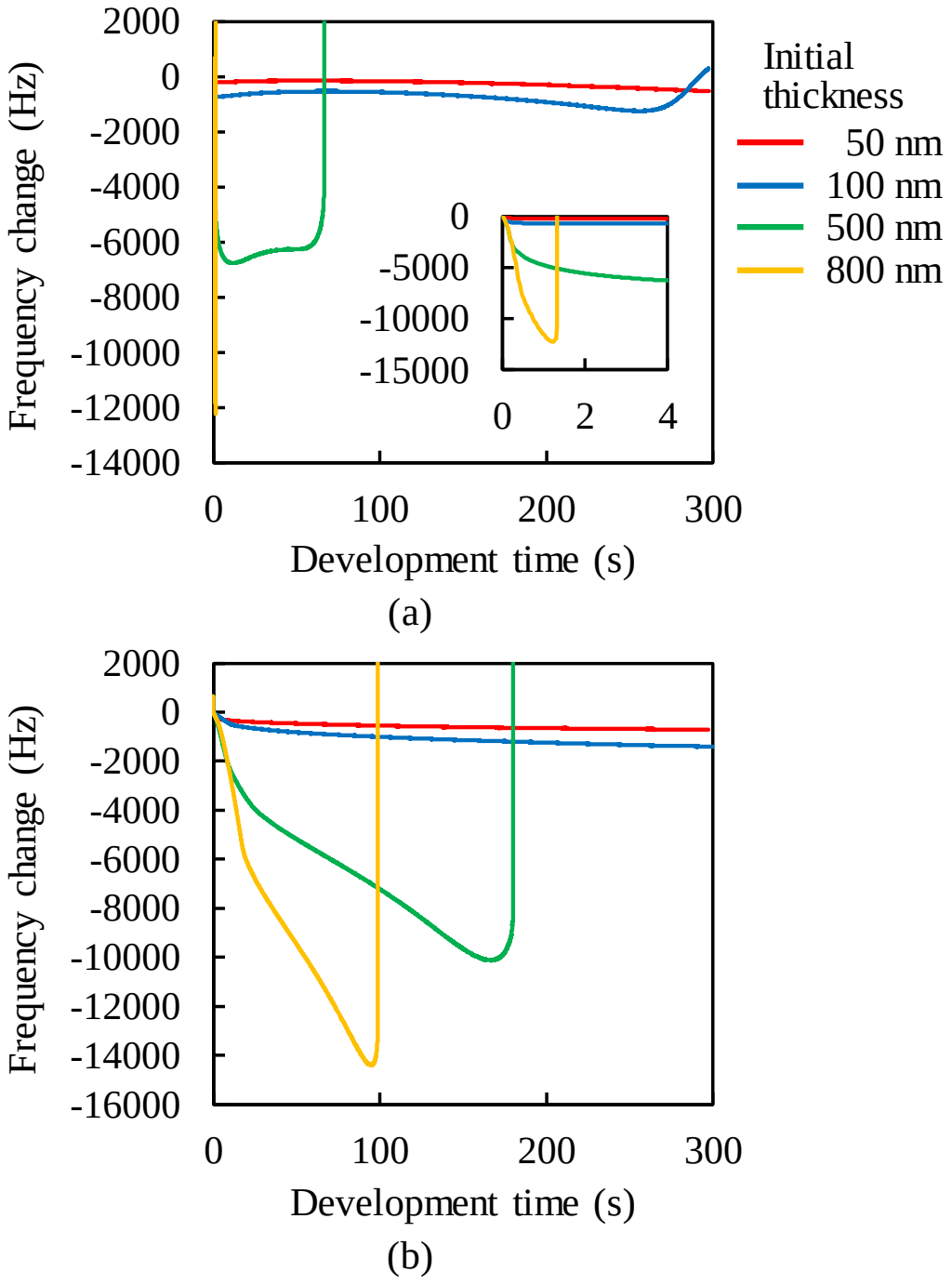

Fig. 2.3. Representative measurement results for the frequency changes of QCM substrates with (a) Polymer-B and (b) C during development. The inset of (a) is the magnified view. The horizontal and vertical axes of the inset represent the development time in s and the frequency change in Hz, respectively.

The impregnated developer was considered to be increased owing to the increase in the acid value, compared with Polymers-A and B. For polymer samples with the initial thicknesses of 500 and 800 nm, the peeling type development was observed. The average time of the onset of peeling and the average frequency reduction for Polymer-B and C are summarized in **Table 2.3**.

Table 2.3. Average dissolution time (or time of peeling onset) and frequency reduction for Polymer-B and C.

Sample	Film thickness (nm)	Dissolution time (s)	Frequency reduction (Hz)
Polymer-B	50	Not dissolved	560.8
	100	295.6	1259.9
	500	55.9*	6802.1
	800	1.4*	12225.5
Polymer-C	50	Not dissolved	714.0
	100	Not dissolved	1647.9
	500	198.0*	10275.0
	800	107.0*	13851.7

*Average time of peeling onset.

The effects of acid values were investigated for further increasing the acid values. **Fig. 2.4(a)** shows the representative measurement results for the frequency changes of QCM substrates with Polymer-D with the acid value of 78 mg KOH/g. For the polymer films with the initial thickness of 800 nm, the frequency decreased until t_{dev} = 5.7 s after the initial drop and increased. From t_{dev} = 7 s, the frequency monotonically increased and became constant after the slight change in the increase rate of frequency. The initial decrease (t_{dev} = 0-5.7 s) and subsequent linear increase (t_{dev} = 7-42 s) in the frequency is characteristics of so-called Case-II diffusion.[19,21,23] They indicate the formation of transient swelling layer (dissolution front) and the steady-state front motion (linear weight loss), respectively. The base-soluble functionality of the polymers used in this study is primarily carboxylic acid units. The schematic dissolution mechanisms of the polymers containing carboxylic acids are as follows.[8,10,11,26]

Firstly, the alkaline aqueous solution penetrates the polymer film to form a thin swelling layer. Secondly, the hydroxyl groups in the swelling layer dissociate. Thirdly, the polymer chains are released from the interaction between polymer molecules in the intermediate gel layer. Finally, the released polymer chains are transferred into the bulk solution. When the initial thickness was decreased, the linear increase region of frequency disappeared at the initial thickness of 100 nm. The frequency reductions were almost same for the polymer films with the initial thickness of 100, 500, and 800 nm, while that for the initial thickness of 50 nm was smaller than the others. These results suggested that the original thickness of the swelling layer before swelling was roughly 100 nm. The increase rate of frequency for 800 nm-thick Polymer-D increased approximately at t_{dev} = 42 s. At this point, the bottom of transient swelling layer was considered to reach the QCM substrate. Therefore, the remaining film consisted of only

swelling layer and this is the reason why the increase rate of frequency increased. The difference between frequencies at the development times of 42 and 60 s was 1457.9 Hz, which corresponds to the mass of 213.9-nm-thick polymer layer if the rigidity of swelling layer is the same as that of initial polymer film. Therefore, the remaining mass (the sum of polymer and impregnated developer) on the QCM substrate is roughly equivalent to that of 213.9 nm-thick polymer layer. In other words, the mass of swelling layer is equivalent to that of 213.9-nm-thick polymer layer approximately at t_{dev} = 42 s. This suggests that the swelling layer significantly expanded. Note that this is rough estimation because the assumption for rigidity is not valid in this case, as previously discussed. It is difficult to define the boundaries between bulk solution and swelling layer and between swelling layer and dry film layer.

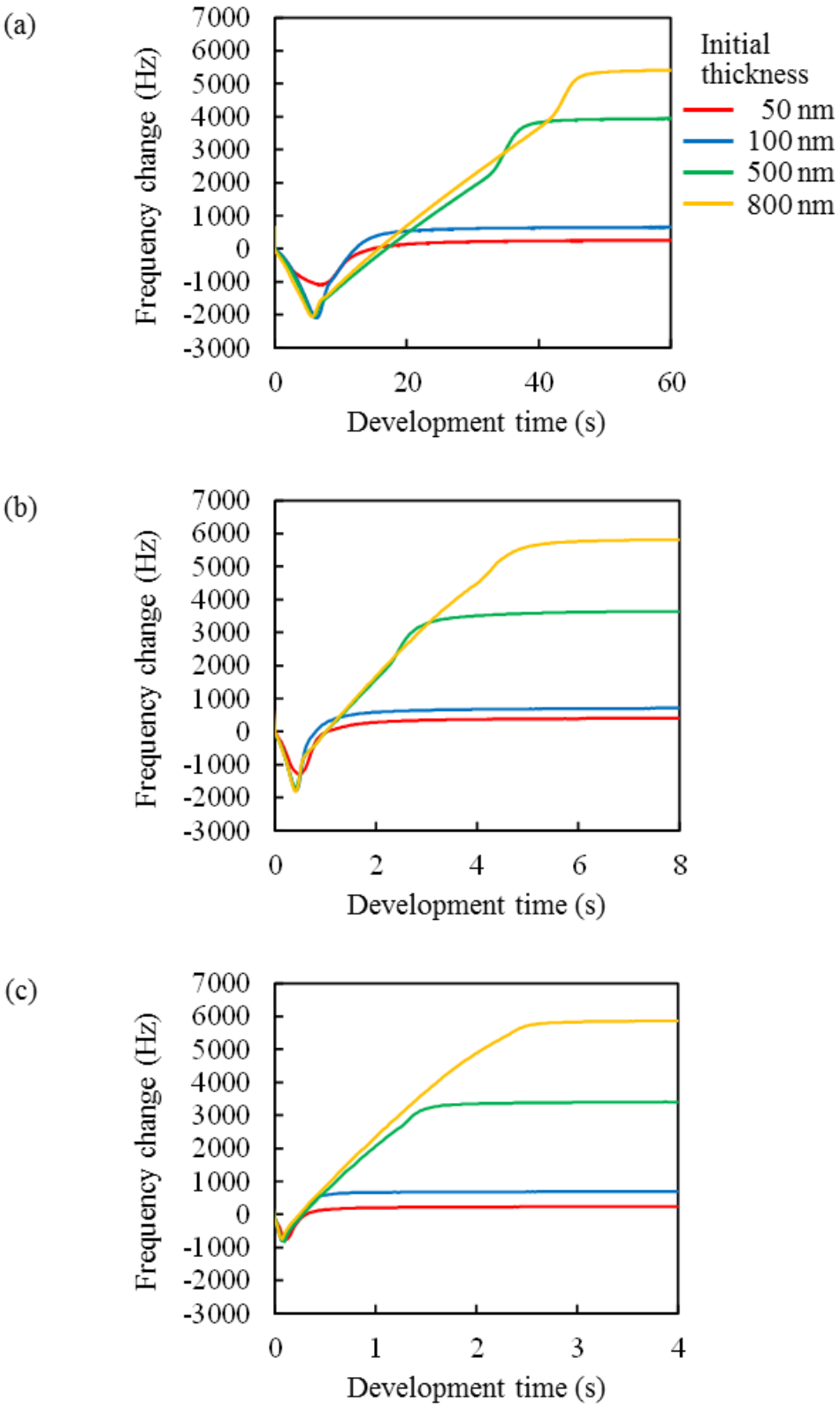

Fig. 2.4. Representative measurement results for the frequency changes of QCM substrates with (a) Polymer-D, (b) E, and (c) F during development.

When the boundary between bulk solution and swelling layer was measured by AFM, two- to three-fold swelling from the original resist thickness was observed.[15] Our consideration described above does not contradict the previous observation with AFM. **Fig. 2.4(b)** shows the representative measurement results for the frequency changes of QCM substrates with Polymer-E with the acid value of 80 mg KOH/g. The base-soluble functionality of the polymers was changed from the monocarboxylic acid units (Polymer-D) to dicarboxylic acid units (tetrahydrophthalic acid), one of hydroxyl group of which was covalently bounded to the polymer side chain, as shown in Fig. 1. pK_a of propionic acids is 4.88.[31] pK_as of tetrahydrophthalic are 3.01 and 5.34.[31] Polymer-E shows the same trend of frequency change as Polymer-D. However, the dissolution time significantly decreased. For the polymer films with the initial thicknesses of 500 and 800 nm, the initial decrease (t_{dev} = 0-0.4 s) and the last increase (t_{dev} = 2.4-3.0 s for 500 nm thickness and t_{dev} = 4.2-5.5 s for 800 nm thickness) just before the complete dissolution in the frequency decreased, compared with Polymer-D. This suggests that the thickness of transient swelling layer became thin. The effect of acid value was examined by increasing the dicarboxylic acid units. **Fig. 2.4(c)** shows the representative measurement results for the frequency changes of QCM substrates with Polymer-F with the acid value of 91 mg KOH/g. The dissolution time was further decreased, compared with Polymer-D and E. The average frequency reductions were almost same for all the polymer films and smaller than those of Polymer-E. Therefore, the original thickness of the swelling layer before swelling was considered to be less than 50 nm. The average dissolution time and the average frequency reductions for Polymer-D, E, and F are summarized in **Table 2.4**

Table 2.4. Average dissolution time and frequency reduction for Polymer-D, E, and F.

Sample	Film thickness (nm)	Dissolution time (s)	Frequency reduction (Hz)
Polymer-D	50	21.4	1083.6
	100	14.6	2054.4
	500	30.4	2031.4
	800	33.7	2085.4
Polymer-E	50	1.6	1290.4
	100	1.2	1791.4
	500	2.3	1659.8
	800	2.8	1794.6
Polymer-F	50	0.5	762.0
	100	0.4	762.5
	500	0.9	823.5
	800	1.2	756.8

2.3.2 The dissolution behaviors of resist films

The dissolution behaviors of resist films were investigated, using Polymer-C, D, and E. **Fig. 2.5** shows the representative measurement results for the frequency changes of QCM substrates with Resist-C. The monomer weight ratio to the sum of polymer and monomer weights was changed from 0 to 75 wt% in steps of 25 wt%. The line marked "0 wt%" is the same as that marked "500 nm" shown in Fig. 3(b). Polymer-C with the

initial thickness of 500 nm showed a peeling type development, as discussed before. When the monomer and photoinitiator were added, Resist-C similarly showed the peeling type development. The time of the onset of peeling became shorter with the increase in the monomer ratio. The frequency reduction also decreased with the increase in the monomer ratio. These results indicate that the interaction between polymers became weak by the addition of low-molecular-weight components. The average time of the onset of peeling and the average frequency reduction for Resist-C are summarized in **Table 2.5.**

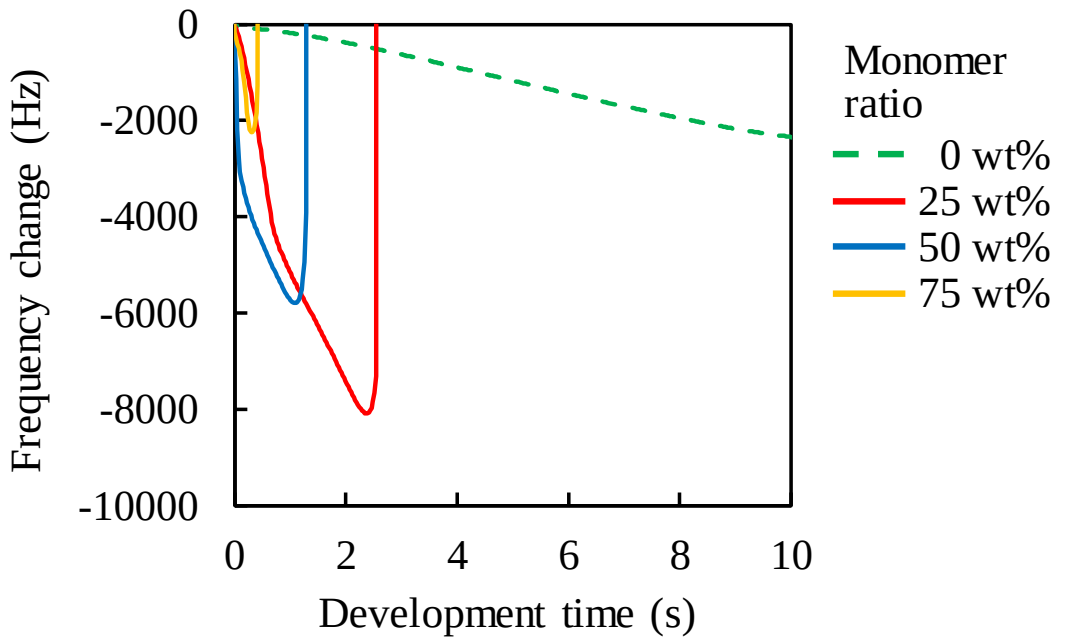

Fig. 2.5. Representative measurement results for the frequency changes of QCM substrates with Resist-C during development.

Table 2.5. Average time of peeling onset and frequency reduction for Resist-C.

Sample	Monomer ratio (wt%)	Onset time (s)	Frequency reduction (Hz)
Resist-C	0	198.0	10275.0
	25	2.7	8050.5
	50	1.4	5824.2
	75	0.5	2438.6

The effects of low-molecular-weight components on the development with Case-II diffusion were investigated. **Fig. 2.6(a)** shows the representative measurement results for the frequency changes of QCM substrates with Resist-D. Resist-D with 25 wt% monomer showed the development with Case-II diffusion. The dissolution time became short, while the average frequency reduction was not significantly changed, compared with Polymer-D. When the monomer weight ratio was increased to 50 and 75 wt%, Resist-D showed the peeling type development**. Fig. 2.6(b)** shows the representative measurement results for the frequency changes of QCM substrates with Resist-E. Resist-E with 25 wt% monomer showed the development with Case-II diffusion, similarly to the case of Resist-D. The dissolution time became short, while the frequency reduction was not significantly changed, compared with Polymer-E. Resist-E with 50 wt% monomer showed the peeling type development. Resist-E with 75 wt% monomer was dissolved without showing the characteristics of swelling, peeling, and Case-II diffusion. The average dissolution time and the average frequency reduction for Resist-D and E are summarized in **Table 2.6**. These effects are also considered to be caused by the weakening of the interaction between polymers through the addition of

low-molecular-weight components.

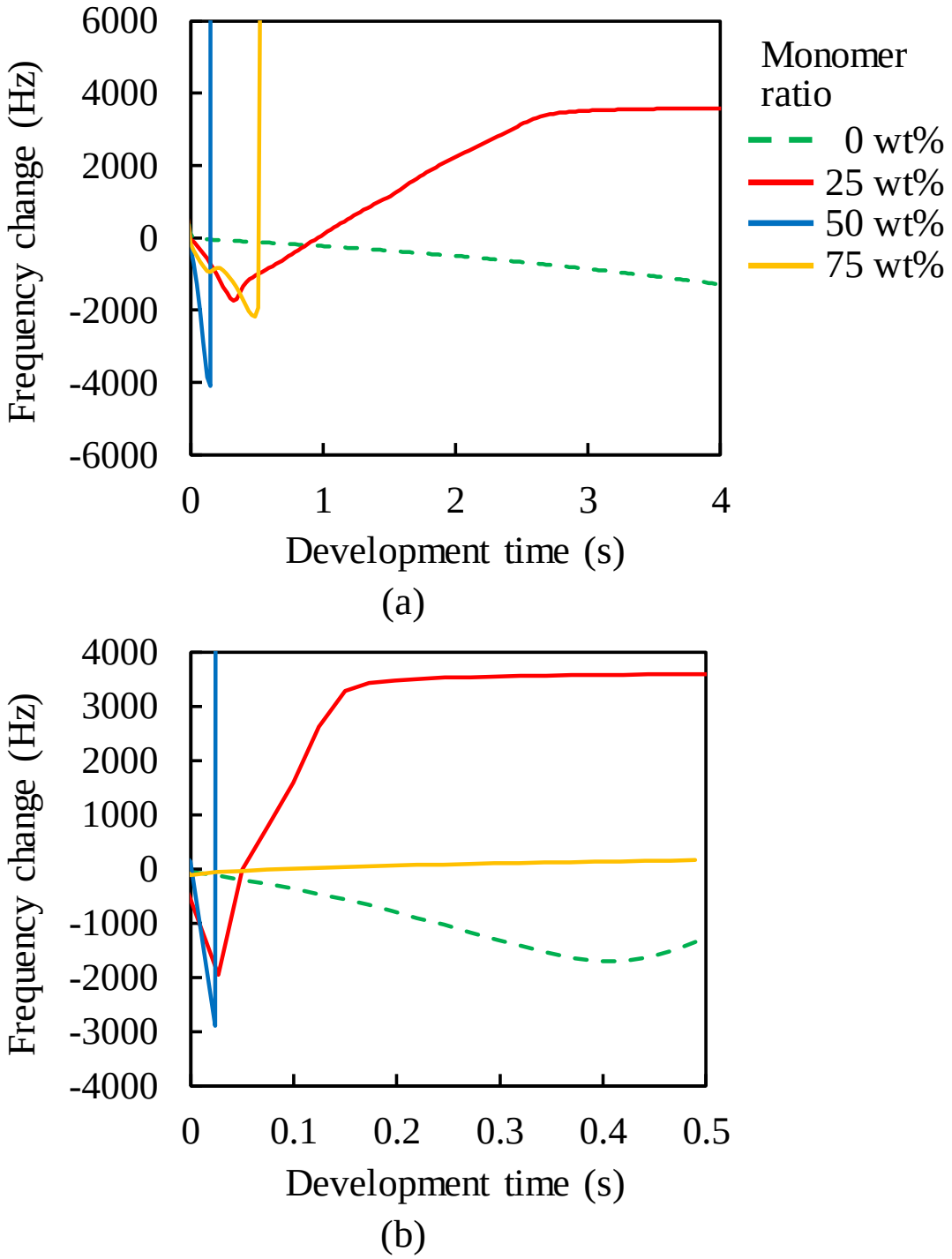

Fig. 2.6. Representative measurement results for the frequency changes of QCM substrates with (a) Resist-D and (b) E during development.

Table 2.6. Average dissolution time and frequency reduction for Resist-D and E.

Sample	Monomer ratio (wt%)	Dissolution time (s)	Frequency reduction (Hz)
Resist-D	0	30.5	2031.4
	25	1.8	1819.9
	50	0.2*	4358.3
	75	0.5*	2283.8
Resist-E	0	2.3	1659.8
	25	0.1	1628.6
	50	0.5*	1498.3
	75	-	-

*Average time of peeling onset.

2.4. Conclusions

In this chapter, the dissolution mechanisms of negative-type resists for the display production were investigated using a QCM method. The frequency change during the development were measured for polymer and resist films. The base-soluble functionality of the polymers used were primarily carboxylic acid units. The resist samples consisted of a polymer, a photosensitizer, a monomer, and a surfactant. The major trend in the effects of acid value on the dissolution behavior was as follows. The development type changed from the insoluble state to the peeling type and the dissolution with Case II diffusion with the increase in acid value. For the dissolution

with Case II diffusion, the dissolution time and swelling layer were decreased with the increase in the acid value. The polarity of polymers, the pK_a of carboxylic acids, the monomer concentration, and the film thickness also affected the dissolution behavior.

References

1) T. Tsuda, Displays **14**, 115 (1993).

2) R.W. Sabnis, Displays **20**, 119 (1999).

3) H. Ito, *Microlithography/Molecular Imprinting* (Springer, Heidelberg, 2005) Advances in Polymer Science Series, Vol. 172, p. 37.

4) H. S. Koo, M. Chen, C. H. Kang, and T. Kawai, Jpn. J. Appl. Phys. **47**, 4954 (2008).

5) C. K. Lee, F. H. Hwang, C. C. Chen, C. L. Chang, and L. P. Cheng, Adv. Polym. Technol. **31**, 163 (2012).

6) J. Thackeray, T. H. Fedynyshyn, D. Kang, M. M. Rajaratnam, G. Wallraff, J. Opitz, and D. Hofer, J. Vac. Sci. Technol. B **14**, 4267 (1996).

7) M. T. Spuller, R. S. Perchuk, and D. W. Hess, J. Electrochem. Soc. **152**, G40 (2005).

8) W. Hinsberg, F. A. Houle, S. W. Lee, H. Ito, and K. Kanazawa, *Macromolecules **38***, 1882 (2005).

9) W. D. Hinsberg, C. G. Willson, and K. K. Kanazawa, J. Electrochem. Soc. **133**, 1448 (1986**)**.

10) M. Toriumi, T. Ohfuji, M. Endo, and H. Morimoto, J. Photopolym. Sci. Technol. **12**, 545 (1999).

11) H. Ito, IBM J. Res. Develop. **45**, 683 (2001).

12) A. Sekiguchi, J. Photopolym. Sci. Technol. **23**, 421 (2010).

13) K. J. Harry, S. Strobel, J. K. W. Yang, H. Duan, and K. K. Berggren, J. Vac. Sci. Technol. B **29**, 06FJ01 (2011).

14) T. Itani and J. J. Santillan, Appl. Phys. Express **3**, 061601 (2010).

15) J. J. Santillan and T. Itani, Jpn. J. Appl. Phys. **51**, 06FC06 (2012).

16) J. J. Santillan and T. Itani, Jpn. J. Appl. Phys. **52**, 06GC01 (2013).

17) T. Itani and T. Kozawa, Jpn. J. Appl. Phys. **52**, 010002 (2013).

18) J. J. Santillan, K. Yamada, and T. Itani, Appl. Phys. Express **7**, 016501 (2014).

19) C. Y. Hui and K. C. Wu, J. Appl. Phys. **61**, 5129 (1987).

20) Y. Tu and A. C. Ouano, IBM J. Res. Develop. **21**, 131 (1977).

21) N. L. Thomas and A. H. Windle, Polym. **23**, 529 (1982).

22) C. A. Mack, J. Electrochem. Soc.: Solid State Sci. Tehnol. **134**, 148 (1987).

23) C. Y. Hui, K. C. Wu, R. C. Lasky, and E. J. Kramer, J. Appl. Phys. **61**, 5137 (1987).

24) T. F. Yeh, H. Y. Shih, and A. Reiser, Macromolecules **25**, 5345 (1992).

25) T. Kudo, Y. Nanjo, Y. Nozaki, H. Yamaguchi, W. B. Kang, and G. Pawlowski, Jpn. J. Appl. Phys. **37**, 1010 (1998).

26) B. Hunek and E. L. Cussler, AIChE J. **48**, 661 (2002).

27) G. Sauerbrey, Z. Phys. **155**, 206 (1959).

28) R. P. Wool, Macromolecules **26**, 1564 (1993).

29) J. L. Parker, P. M. Claesson, and P. Attard, J. Phys. Chem. **98**, 8468 (1994).

30) A. Faghihnejad and H. Zeng, Soft Matter **8**, 2746 (2012).

31) H. C. Brown *et al*. in *Determination of Organic Structures by Physical Methods* eds. E. A. Braude and F.C. Nachod (Academic Press, New York, 1955).

Chapter 3

Relationship between C=C double bond conversion and dissolution kinetics in cross-linking-type photoresists for display manufacture, studied by real-time Fourier transform infrared spectroscopy and quartz crystal microbalance methods

3.1. Introduction

In the application of photoresists to micro- and nanofabrication, the control of the resist pattern shape is an important issue. In particular, the development process of photoresists is essential because it significantly affects the resist pattern formation. The development process has been investigated by various methods [1-14] The author also reported the dissolution kinetics of unexposed polymer and resist films in chapter 2.[9] The changes in the frequency of a QCM during photoresist development have been measured for polymer and resist films. The major trend observed was as follows. The development type changed from an insoluble type to the peeling type and the dissolution type with Case II diffusion with increasing acid value of the polymers. The dissolution with Case II diffusion is characterized by the formation of a transient swelling layer (dissolution front) and steady-state front motion (linear weight loss). For dissolution with Case II diffusion, the dissolution time and the original thickness of the transient swelling layer decreased with increasing acid value of polymers.[9] Note that the acid value is described as the weight (mg) of potassium hydroxide (KOH) required

to neutralize the acidic component contained in 1 g of a polymer.

In cross-linking-type photoresists, dissolution kinetics depend on the degree of cross-linking. UV curing processes have been investigated by IR spectroscopy, [15-17] Raman spectroscopy,[18] ESR,[19] and UV rheometry.[20] However, the details of the relationship between cross-linking and dissolution kinetics are unknown. In this chapter, the author demonstrated the development process of cross-linking-type photoresists used for display manufacture. The C=C double bond conversion induced upon exposure to UV light was measured by a real-time Fourier transform infrared spectroscopy (FTIR) method. The dissolution behavior of exposed photoresists in a TMAH aqueous developer was measured using a QCM. The shapes of resist patterns after development were observed by scanning electron microscopy (SEM). The relationship between C=C double bond conversion and dissolution kinetics is discussed.

3.2. Experimental

Two kinds of polymers and two kinds of photoinitiators, 1,2-octanedione-1-[4-(phenylthio)-2-(*O*-benzoyloxime)]and bis(2,4,6-trimethylbenzoyl)-phenylphosphine oxide, were used, as shown in **Fig. 3.1**. These photoinitiators used as purchased (BASF).

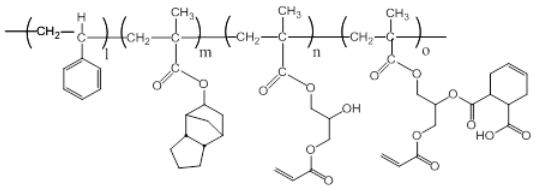

0.05 0.02 0.83 0.1

Polymer-B

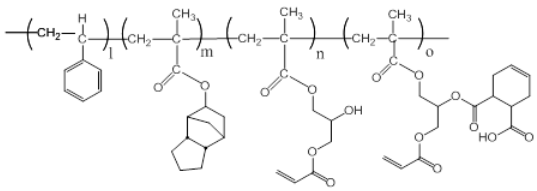

0.1 0.3 0.21 0.39

Polymer-E

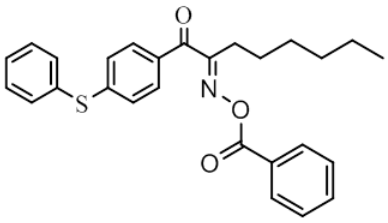

PI-1

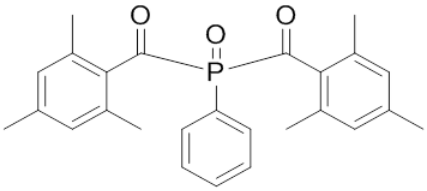

PI-7

Fig. 3.1. Molecular structures of polymers and photoinitiators used. PI-1and PI-7 are 1,2-octanedione-1-[4-(phenylthio)-2-(O-benzoyloxime)] and bis(2,4,6-trimethylbenzoyl) -phenylphosphine oxide), respectively.

The molecular weights and acid values of the polymers are listed in **Table 3.1.** The resist samples consisted of a polymer (Polymer-B or Polymer-E), a monomer, a photoinitiator (PI-1 or PI-7), and a surfactant. Di-pentaerythritol polyacrylate was used as a monomer. The weight ratio of each polymer to the monomer was 1:1. The concentration of the photoinitiator was adjusted so that the conversion ratio of C=C double bonds was approximately 0.5 upon exposure to 50 mJ/cm^2 UV light under N_2 purging for each photoresist. A fluorochemical surfactant was used for uniform film formation. The surfactant concentration was 0.1 wt%. Four kinds of photoresists were prepared by mixing the resist components, as listed in **Table 3.2.** The resist samples were dissolved in propyleneglycol monomethyl ether acetate (PGMEA) before

spin-coating.

Table 3.1. Molecular weights (Mw) and acid values of polymers.

Sample	Mw	Acid value (mg KOH/g)
Polymer-B	9000	30
Polymer-E	8400	80

Table 3.2. Resist components and photoinitiator concentrations. Numerical values in the brackets in the rightmost column represent the concentrations of photoinitiators in wt%.

Resist	Polymer	Photoinitiator
Resist-B1	Polymer-B	PI-1 (2)
Resist-B2	Polymer-B	PI-1 (5)
Resist-E1	Polymer-E	PI-7 (3)
Resist-E2	Polymer-E	PI-7 (10)

In real-time FTIR(Bruker-Optics VERTEX 70) experiments, resist solutions were spin-coated on silicon substrates and baked at 100 °C for 60 s to form resist films with a thickness of 0.5 μm. The baking temperature was slightly elevated, compared with those in QCM and patterning experiments, to obtain uniform films. It was confirmed by differential scanning calorimetry that no thermal polymerization occurred under the baking condition. The resist films were exposed to UV light with a wavelength of 365 nm from a mercury lamp (EXFO Omnicure^{TM} S2000) and an intensity of 1 mW/cm^2. The samples were exposed to UV light in the atmosphere or under N_2 purging. The

exposure dose was set to 50 mJ/cm^2. FTIR measurement was carried out under UV light exposure condition using a real-time FTIR system (Bruker-Optics VERTEX 70). The details of the measurement system and procedure have been reported elsewhere.[21,22] The C=C double bond conversion of resist samples during UV light exposure was calculated by dividing the absorbance peak height at 812 cm^{-1} (CH out-of-plane bending band) by the initial absorbance peak height before UV light exposure.

In the QCM experiments, resist solutions were spin-coated on QCM substrates and baked at 90 °C for 120 s to form resist films with a thickness of 0.5 μm. The resist films were exposed to UV light from a UV lamp (AS ONE Handy UV Lamp SLUV6) in the atmosphere. The wavelength and light intensity were 365 nm and 0.86-0.98 mW/cm^2, respectively. The exposure doses were 0, 5,10, 20, 30, 40, and 50 mJ/cm^2. The dissolution kinetics of resist films were investigated using a QCM-based development analyzer (Litho Tech Japan RDA-Qz3).[5] 2.38% TMAH aqueous solution (Tokyo Ohka Kogyo NMD-3) was used as an aqueous base developer. For a thin, rigid film applied to a crystal surface, the frequency shift ΔF linearly increases with increasing mass of the applied film[3, 25]

$$\Delta F = -\frac{2F_0^2}{\sqrt{\rho_Q \mu_Q}} m' \qquad (3-1)$$

Here, F_0 is the resonant frequency at the unloaded QCM substrate, m' is the mass of the film, ρ_Q is the density of the quartz crystal, and μ_Q is its shear modulus corrected for piezoelectric stiffening.

In the patterning experiments, line patterns were fabricated. The width of lines on the mask was 20 μm. Resist solutions were spin-coated on glass substrates, dried under

reduced pressure, and baked at 90 °C for 120 s to form resist films with a thickness of 0.5 μm. The resist films were exposed to UV light using the exposure system with a deep-UV-cut filter (Japan Science Engineering MA-1100) in the atmosphere. The wavelength of the light was 365 nm. The exposure intensity and dose were 45 mW/cm^2 and 50 mJ/cm^2, respectively. The exposed samples were developed in 2.38% TMAH aqueous solution (Parker Corporation PK-DETX2250) for 80 s using a puddle-type developing machine. The resist patterns after development were observed by SEM (Hitachi SU1510).

3. 3 Results and discussion

3.3.1 Comparison of C=C double bond conversion and dissolution kinetics of Polymer-B

The C=C double bond conversion of Resists A and B during UV light exposure was evaluated by real-time FTIR. The polymer of Resists B1 and B2 was Polymer-B. The acid value of Polymer-B was 30 mg KOH/g. Upon exposure to UV light, PI-1 and PI-7 decomposed to radical species. The decomposition processes have been reported.[24-26)] The major radicals generated are shown in **Fig. 3.2**. These radicals induce cross-linking.

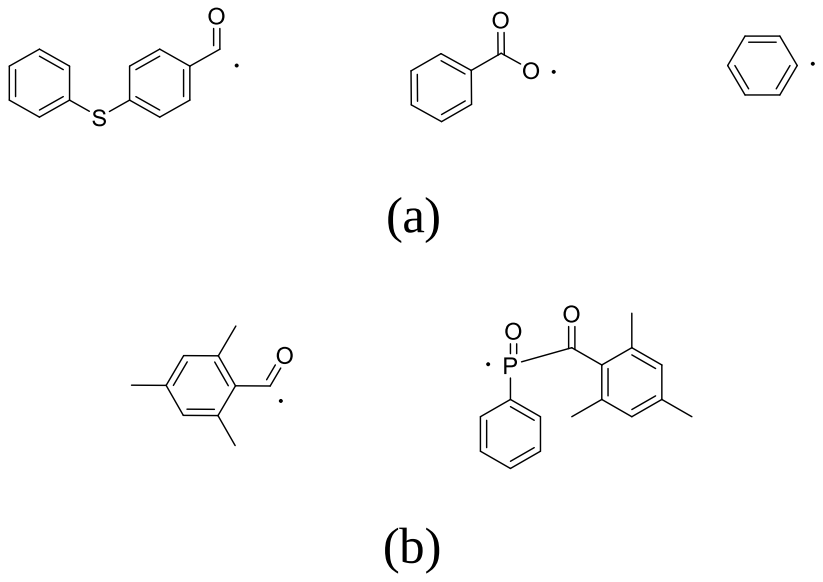

Fig. 3.2. Estimated major radicals generated through the decomposition of (a) PI-1 and (b) PI-7 upon exposure to UV light.

The temporal changes in the conversion ratio during the exposure to UV light in the atmosphere and under N_2 purging are shown in Fig.3.3. The concentrations of the photoinitiators were adjusted so that the conversion ratio of Resist-B2 agreed with that of Resist-B1 under N_2 purging, as described in Sect. 3.2. It has been reported that the cross-linking is inhibited by oxygen through radical scavenging.[22] The effect of oxygen inhibition in Resist-B1 was larger than that in Resist-B2. The reactivity of radicals generated from PI-1 with oxygen [**Fig. 3.2(a)**] was higher than that of radicals generated from PI-7 [**Fig. 3.2(b)**] in comparison with their respective reactivities with C=C double bonds. The details of the dissolution kinetics of a 0.5-μm-thick film of Polymer I without any additives have been investigated.[9] The dissolution of the Polymer-B film was of the peeling type owing to its low acid value. The dissolution kinetics of the photoresists with Polymer I were investigated.

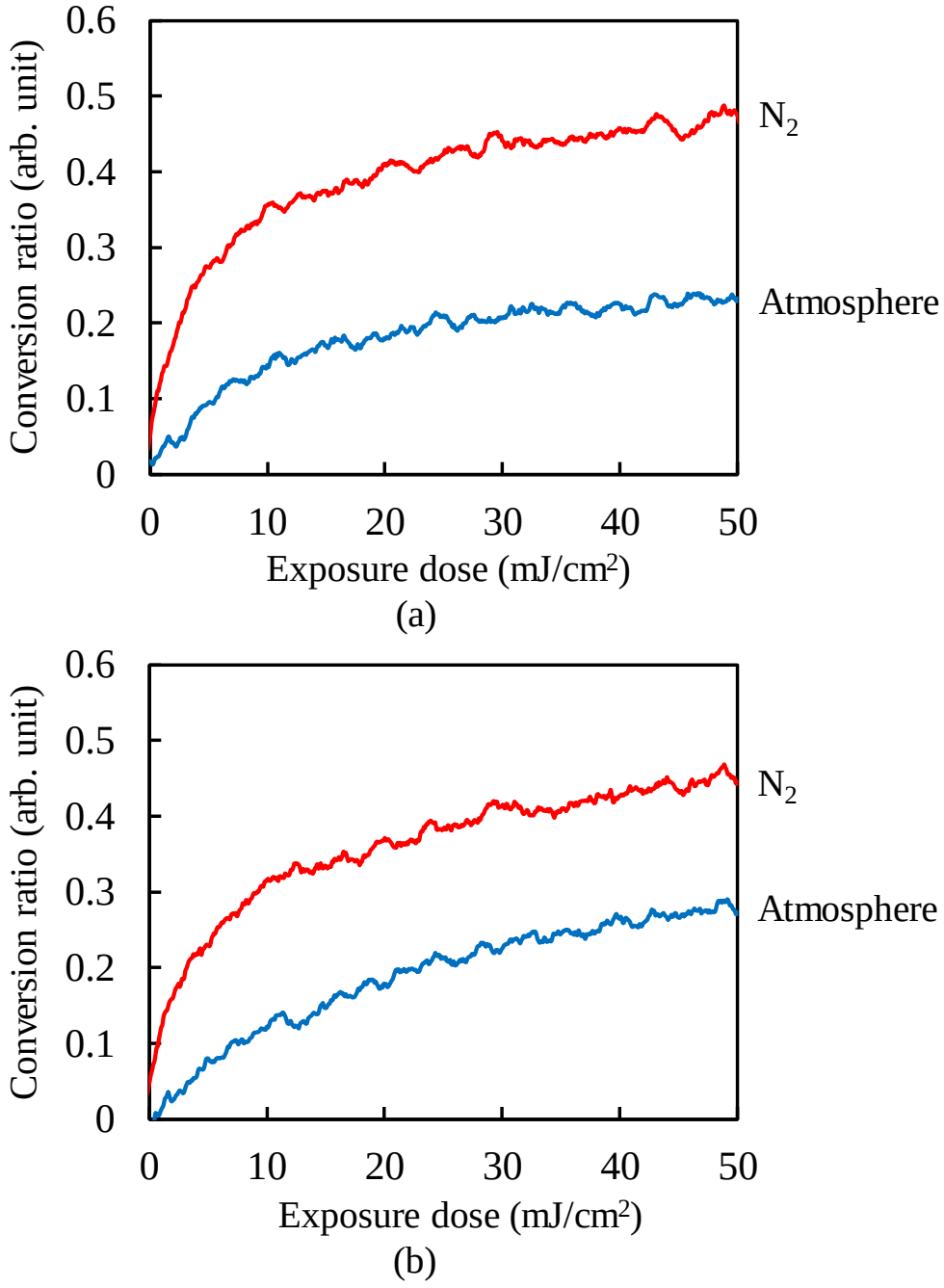

Fig. 3.3. Temporal changes in conversion ratio of C=C double bonds for (a) Resist-B1 and (b) B2 during the exposure to UV light in the atmosphere and under N_2 purging.

Fig. 3.4 shows the frequency changes of QCM substrates with Resist-B1 and Resist-B2 exposed to UV light in the atmosphere, namely, in the presence of oxygen.

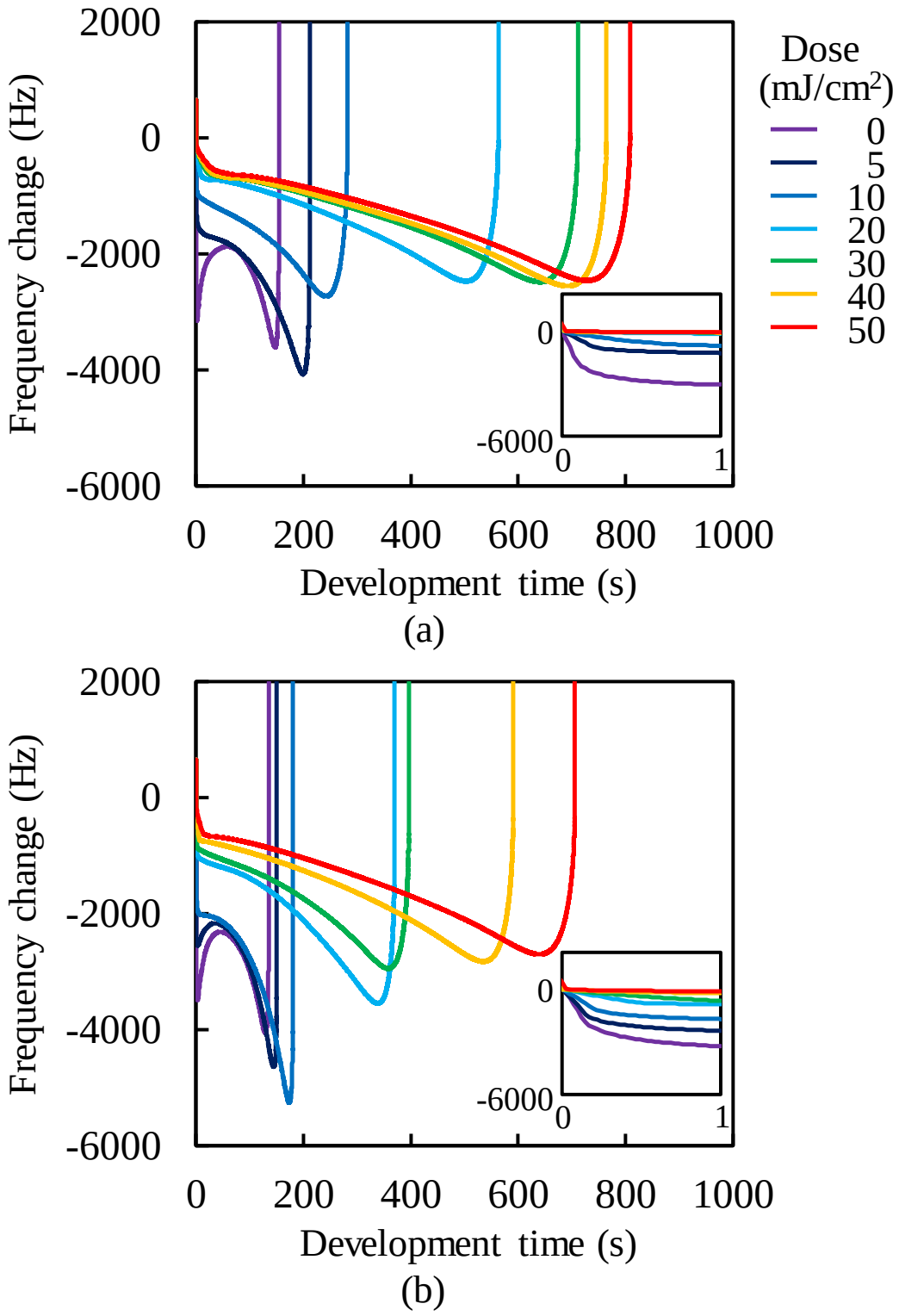

Fig. 3.4. Frequency changes of QCM substrates with (a) Resist-B1 and (b) B2 during development. The insets are magnified views. The horizontal and vertical axes of the insets represent the development time in s and the frequency change in Hz, respectively.

Upon the insertion of QCM substrates into the developer, the frequency immediately dropped by approximately 660 Hz owing to the increase in the viscosity of their surroundings. The frequency immediately after the drop was set to 0 (a base) and the frequency change was plotted in the graph. The line marked "0" in **Fig. 3.4**(a) represents the dissolution kinetics of unexposed Resist-B1. After the initial drop, the frequency immediately decreased by approximately another 3200 Hz. This decrease in the frequency is due to the increase in the mass of the polymer films, as indicated by Eq. (3－1). The increase in the mass was caused by the penetration of the developer into the resist film. The premise of Eq. (3－1) is that the film is rigid. However, the penetration of the developer softens the resist film.[9)] Therefore, I should regard Eq. (3－1) as a rough estimation when the swelling layer increases in thickness. Also, the frequency increased from 1.6 to 60 s. This increase is considered to be caused by the softening of the resist film. From 60 to 145 s, the frequency decreased. Owing to the softening of the resist film, the penetration of the developer into the resist film is considered to have accelerated. At 154 s, the frequency abruptly rose and started to strongly fluctuate, which was omitted from the graph to clearly display the results. The fluctuation indicates that the dissolution of these polymer films was not smooth and that the polymer layer peeled off as microscopic flakes as a result of the shear force.[9,27)] The line marked "5" in **Fig. 3.4(a)** represents the dissolution kinetics of Resist A after being exposed to 5 mJ/cm^2 UV light. The double bond conversion ratio was 0.10, as shown in Fig. 3(a). The initial intake of the developer from 0 to approximately 10 s was slower than that of the unexposed photoresist. The negative peak immediately after the insertion disappeared with the slowdown of developer intake. With the progress of

development, the rate of decrease in the frequency decreased and then increased after approximately 10 s (inflection point). After the inflection point at 10 s, the frequency gradually decreased to -4073 Hz. At the double bond conversion ratio of 0.10, the negative maximum of the frequency change (absolute value) of the exposed photoresist was greater than that of the unexposed photoresist. This suggests that the degree (frequency change) of developer impregnation shortly before the onset of peeling (the impregnation threshold) increased as a result of the cross-linking. After the inflection point, the rate of decrease in the frequency gradually increased with the development time. The intake rate of the developer is considered to have increased owing to the softening of the resist film. The average rate of decrease in the frequency of the exposed photoresist after the inflection point was lower than that of the unexposed photoresist owing to the cross-linking. The onset of peeling was also delayed owing to the cross-linking. For the exposure doses larger than 5 mJ/cm^2, the dissolution behavior was similar to that for 5 mJ/cm^2. The rate of decrease in the frequency before the onset of peeling decreased with increasing exposure dose. The onset of peeling was also delayed with increasing exposure dose. The impregnation threshold decreased at the double bond conversion of 0.14 (at the exposure dose of 10 mJ/cm^2) and became approximately constant from 0.18 (at the exposure dose of >20 mJ/cm^2).

Fig. 3.4(b) shows the dissolution kinetics of Resist-B2 exposed to UV light in the atmosphere. The trend in the relationship between the dissolution kinetics and conversion ratio was similar to that observed in Resist-B1. The difference between Resist-B1 and Resist-B2 is next discussed. The impregnation threshold for Resist-B2 was higher than that for Resist-B1 on the whole. This is considered to be caused by the differences in the concentration and molecular structure of the photoinitiators because

the impregnation threshold of unexposed Resist-B2 was higher than that of unexposed Resist-B1. For the rate of developer intake, the rate of decrease in the frequency before the inflection point in exposed Resist-B2 was higher than that in exposed Resist-B1. The negative peak immediately after the insertion disappeared at the conversion ratio of 0.12 (at the exposure dose of 10 mJ/cm2), which was larger than that in the case of Resist-B1. The development time at the inflection point was earlier in Resist-B2 than in Resist-B1. The rate of decrease in the frequency after the inflection point was also higher in Resist-B2. These results suggest that the rate of developer intake in Resist-B2 is higher than that in Resist-B1. However, this contradicts the observation that the double bond conversion in Resist-B2 is higher than that in Resist-B1. This disagreement was caused by the difference of the radicals generated through the decomposition of photoinitiators, because the rate of developer intake of unexposed Resist-B2 was lower than that of unexposed Resist-B1.

Fig. 3.5 shows SEM images of the cross sections of resist patterns fabricated with Resist-B1 and Resist-B2. The heights of the resist patterns were 0.40 and 0.28 μm for Resist-B1 and Resist-B2, respectively. The line widths at the top of the resist patterns were 16.2 and 15.0 μm, and those at the bottom of the resist patterns were 18.7 and 17.2 μm for Resist-B1 and Resist-B2, respectively. The taper angles were 11.1 and 6.3° for Resist-B1 and Resist-B2, respectively. Regarding the contradiction between dissolution kinetics and double bond conversion discussed previously, the observed images support our discussion of the dissolution kinetics (the exposed Resist-B2 dissolves more easily than the exposed Resist-B1). However, the development time in the patterning experiment was 80 s. In the QCM experiments, even the unexposed photoresists did not dissolve within 80 s. This difference is considered to have been caused by the difference

in the interaction between photoresists and substrates. Glass substrates were used for the patterning experiments. In the QCM experiments, the photoresists were spin-coated on gold electrodes on the QCM substrates. The peeling-type dissolution was considered to start earlier on the glass substrates than on the QCM substrates owing to the weak interaction between the glass substrates and photoresists. It is also possible that the patterned structures of the photoresists induced additional mechanical stress and

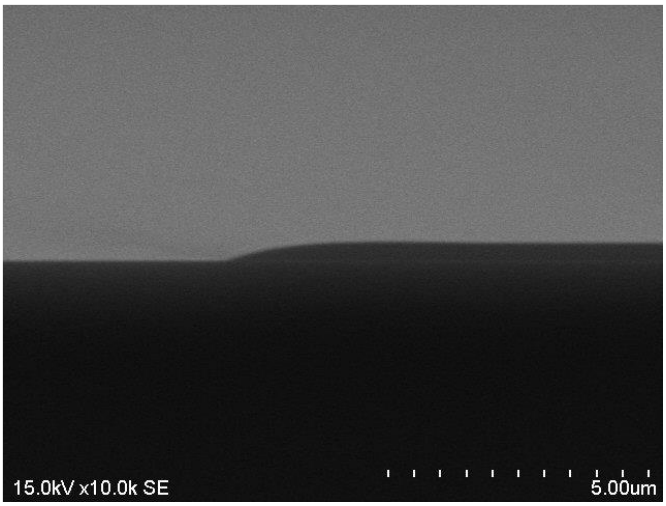

(a)

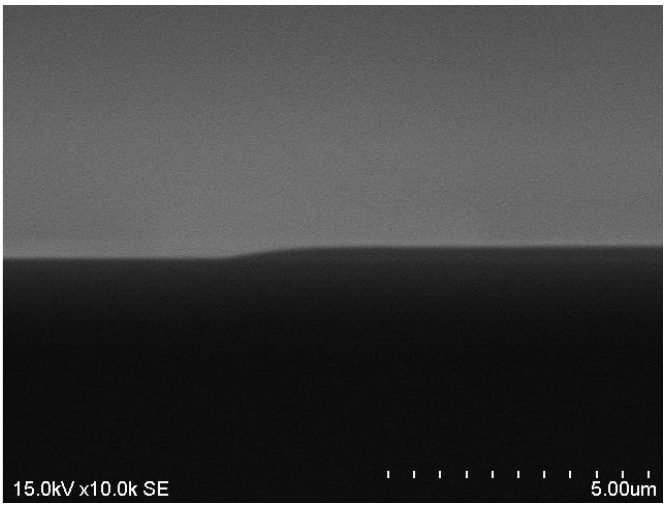

(b)

affected the timing of the peeling in the patterning experiments.

Fig. 3.5. SEM images of the cross sections of resist patterns fabricated with (a) Resist-B1 and (b) B2.

3.3.2 Comparison of C=C double bond conversion and dissolution kinetics of Polymer-E

The dissolution kinetics of photoresist films with Polymer-E was investigated. Unlike Polymer-B, a 0.5 μm-thick film of Polymer-E without any additives shows the dissolution type with Case II diffusion, mainly owing to its high acid value.[9] The acid value of Polymer-B was 80 mg KOH/g. **Fig. 3.6** shows the temporal changes in the conversion ratio during the exposure to UV light in the atmosphere and under N_2 purging. Despite the large difference in the polymer structures, in particular, the acid value and double bond content, the effects of oxygen inhibition in the photoresists with Polymer-E did not significantly differ from those in the photoresists with Polymer-B for each photoinitiator. The dissolution kinetics of Resist-E1 is shown in **Fig. 3.7(a)**. The polymer changed from the dissolution type with Case II diffusion to the peeling type by adding resist components such as a monomer. For the unexposed photoresist, the initial decrease in the frequency and its rate of decrease were greater than those for Resist-B1. The intake of developer in the unexposed photoresist was faster than that in Resist-B1 owing to the high acid value. No second negative peak was observed, unlike in the case of unexposed Resist-B1. Peeling started without any noticeable softening of the resist films, which was observed in the cases of Resist-B1 and Resist-B2. For the exposed photoresists, the frequency gradually decreased after the rapid decrease and then the peeling started. The rate of decrease in the frequency basically decreased with development time, which is in significant contrast to the photoresists with Polymer-B.

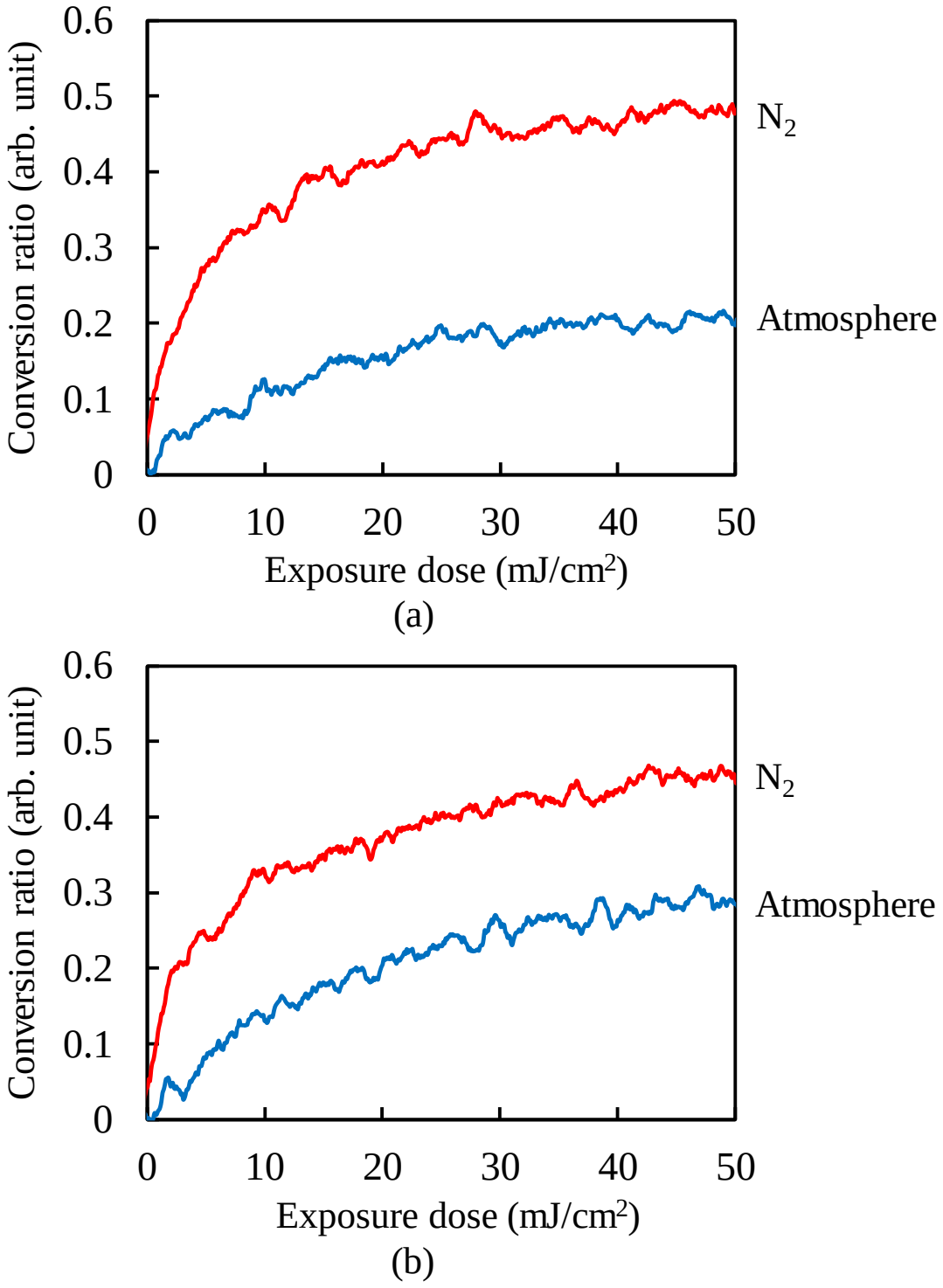

Fig. 3.6. Temporal changes in conversion ratio of C=C double bonds for (a) Resist-E1 and (b) E2 during the exposure to UV light in the atmosphere and under N_2 purging.

This suggests that the developer intake tends to saturate with development time. **Fig. 3.7(b)** shows the dissolution kinetics of Resist-E2. Note that the scale of the horizontal axis of **Fig. 3.7(b)** is significantly different from that of **Fig. 3.7(a)**. The impregnation threshold of Resist-E2 was generally higher than that of Resist-E1. This is considered to be caused by the differences in the concentration and molecular structure of the photoinitiators because the impregnation threshold of unexposed Resist-E2 was higher than that of unexposed Resist-E1, similarly to the case of the photoresists with Polymer-B. At an exposure dose higher than 10 mJ/cm^2, the rate of decrease in the frequency in Resist-E2 was higher than that in Resist-E1. The onset of peeling in Resist –E2 was also earlier than that in Resist-E1. These results suggest that the rate of developer intake in Resist-E2 is higher than that in Resist-E1 at an exposure dose higher than 10 mJ/cm^2. However, this contradicts the finding that the double bond conversion in Resist-E2 is higher than that in Resist-E1. This disagreement was considered to be caused by the difference of the radicals generated through the decomposition of photoinitiators, similarly to the case of the photoresists with Polymer-B. On the whole, the impregnation threshold in the photoresists with Polymer-E was higher than that in the photoresists with Polymer-B. This is considered to be due to the hydrophobic interaction of Polymer-E being stronger than that of Polymer-B.

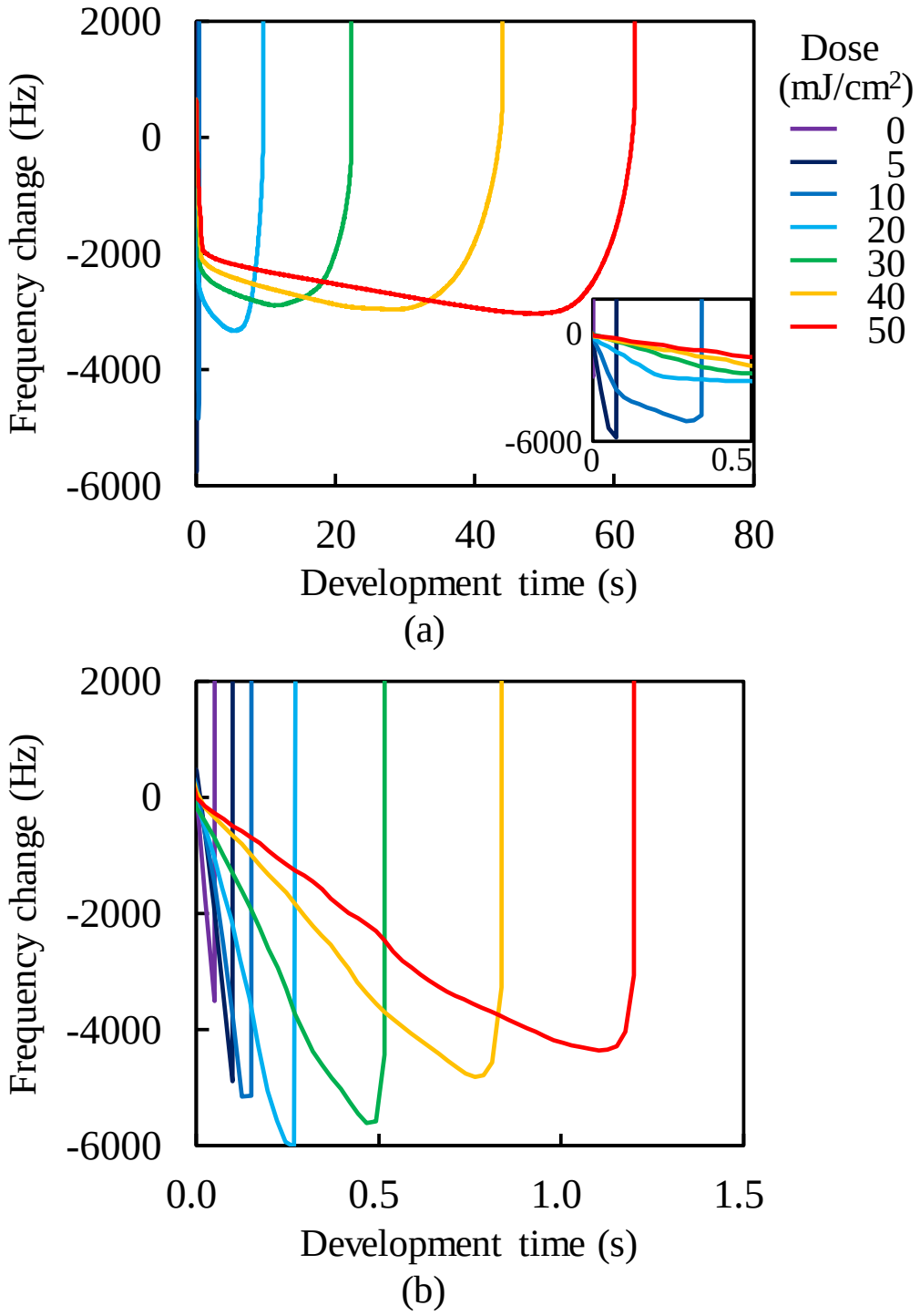

Fig. 3.7. Frequency changes of QCM substrates with (a) Resist-E1 and (b) E2 during development. The inset of (a) is a magnified view. The horizontal and vertical axes of the inset represent the development time in s and the frequency change in Hz, respectively. The onset time of peeling and the impregnation threshold for the unexposed Resist C were 25 ms and -2365 Hz, respectively.

In the patterning experiments, Resist-E1 dissolved and the resist pattern was not resolved. The peeling off of resist patterns from the substrate was observed in Resist-E2. **Fig. 3.8** shows an SEM image of a cross section of a resist pattern fabricated with Resist-E2. The height of the resist pattern was 0.18 μm. The line widths at the top and bottom of the resist pattern were 14.6 and 16.0 μm, respectively. The taper angle was 12.8°.

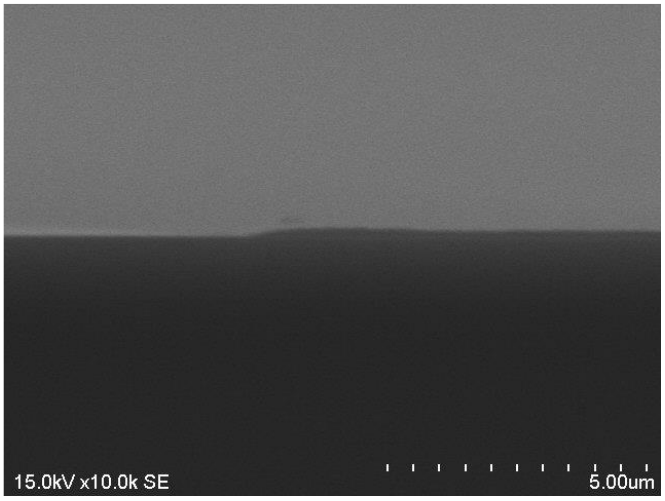

Fig. 3.8. SEM image of the cross section of the resist pattern fabricated with Resist-E2.

3.4. Conclusions

The exposure dose dependence of the dissolution of cross-linking-type photoresists for display manufacture was investigated using the real-time FTIR and QCM methods. Two kinds of polymers (Polymer-B with peeling-type dissolution and Polymer-E with a dissolution type with Case II diffusion) and two kinds of photoinitiators were used. For both polymers, the dissolution type became the peeling type when they were formulated as a typical negative-type photoresist. With increasing conversion ratio of double bonds, the penetration rate of developer decreased and the impregnation threshold increased

and then decreased. For Polymer-B, the impregnation threshold became constant with a sufficient exposure dose. The effect of oxygen inhibition for PI-1 was larger than that for PI-7. Although the conversion ratio in the photoresists with PI-1 was lower than that in the photoresists with PI-7, the rate of developer intake in the photoresists with PI-1 was lower than that in the photoresists with PI-7. This disagreement was considered to be caused by the difference of the radicals generated through the decomposition of photoinitiators.

References

1) J. Thackeray, T. H. Fedynyshyn, D. Kang, M. M. Rajaratnam, G. Wallraff, J. Opitz, and D. Hofer, J. Vac. Sci. Technol. B **14**, 4267 (1996).

2) M. T. Spuller, R. S. Perchuk, and D. W. Hess, J. Electrochem. Soc. **152**, G40 (2005).

3) W. Hinsberg, F. A. Houle, S. W. Lee, H. Ito, and K. Kanazawa, Macromolecules **38**, 1882 (2005).

4) W. D. Hinsberg, C. G. Willson, and K. K. Kanazawa, J. Electrochem. Soc. **133**, 1448 (1986).

5) M. Toriumi, T. Ohfuji, M. Endo, and H. Morimoto, J. Photopolym. Sci. Technol. **12**, 545 (1999).

6) H. Ito, IBM J. Res. Dev. **45**, 683 (2001).

7) A. Sekiguchi, J. Photopolym. Sci. Technol. **23**, 421 (2010).

8) K. J. Harry, S. Strobel, J. K. W. Yang, H. Duan, and K. K. Berggren, J. Vac. Sci. Technol. B **29**, 06FJ01 (2011).

9) A. Tsuneishi, S. Uchiyama, and T. Kozawa, Jpn. J. Appl. Phys. **57**, 046501 (2018).

10) T. Itani and J. J. Santillan, Appl. Phys. Express **3**, 061601 (2010).

11) J. J. Santillan and T. Itani, Jpn. J. Appl. Phys. **51**, 06FC06 (2012).

12) J. J. Santillan and T. Itani, Jpn. J. Appl. Phys. **52**, 06GC01 (2013).

13) T. Itani and T. Kozawa, Jpn. J. Appl. Phys. **52**, 010002 (2013).

14) J. J. Santillan, K. Yamada, and T. Itani, Appl. Phys. Express **7**, 016501 (2014).

15) C. Decker, Polym. Int. **51**, 1141 (2002).

16) P. M. Johnson, J. W. Stansbury, and C. N. Bowman, Macromol. React. Eng. **3**, 522 (2009).

17) K. S. Anseth, C. M. Wang, and C. N. Bowman, Macromolecules **27**, 650 (1994).

18) M. Schmitt, RSC Adv. **4**, 1907 (2014).

19) M. Schmitt, Analyst **138**, 3758 (2013).

20) C. A. Bonino, J. E. Samorezov, O. Jeon, E. Alsberg, and S. A. Khan, Soft Matter **7**, 11510 (2011).

21) K. Taki, T. Taguchi, R. Hayashi, and H. Ito, J. Photopolym. Sci. Technol. **29**, 133 (2016).

22) K. Taki, Y. Watanabe, H. Ito, and M. Ohshima, Macromolecules **47**, 1906 (2014).

23) G. Sauerbrey, Z. Phys. **155**, 206 (1959) [in German].

24) Y. Muramatsu, M. Kaji, A. Unno, and O. Hirai, J. Photopolym. Sci. Technol. **23**, 447 (2010).

25) D. E. Fast, A. Lauer, J. P. Menzel, A.-M. Kelterer, G. Gescheidt, and C. Barner-Kowollik, Macromolecules **50**, 1815 (2017).

26) K. Ikemura and T. Endo, Dental Mater. J. **29**, 481 (2010).

27) B. Hunek and E. L. Cussler, AIChE J. **48**, 661 (2002).

Summary

In chapter 1, the author developed a novel experimental method, which evaluates the radical generation yield of photo initiators upon UV irradiation using galvinoxyl radical as an indicator. The absolute quantum efficiency of free radical generation was determined by this method for six different photo initiators. The yields were in good agreement with the results of the theoretical calculations, where the rate of intersystem crossing was revealed to be the determinant step for the resultant radical generation yield. It was suggested that the efficiency of intersystem crossing is important in the molecular design for the enhancement of the quantum yield.

In chapter 2, the author investigated the dissolution behavior of negative-type photoresists for display manufacturing by QCM. The frequency changes during the development were measured for polymer and resist films. The observed major trend was as follows. The development type changed from an insoluble state to a peeling type with the increase in the acid value of polymers or the decrease in the hydrophobicity of polymer. The dissolution behavior showed Case II diffusion when the acid value of polymer further increased. For the dissolution with Case II diffusion, the dissolution time and the original thickness of transient swelling layer were decreased with the increase in the acid value of polymers.

In chapter 3, the author clarified the relationship between C=C double bond conversion and dissolution behavior in the cross-linking-type resists used for display manufacture using real-time FTIR and QCM. To improve the resist shape, it is important to understand the development mechanism. Two kinds of polymers (a polymer with

peeling-type dissolution and a polymer with a dissolution type with Case II diffusion) were used. 1,2-octanedione-1-[4-(phenylthio)-2-(O-benzoyloxime)] and bis(2,4,6-trimethylbenzoyl)-phenylphosphine oxide were used as photoinitiators. The dissolution was of the peeling type when the polymers were formulated as a typical cross-linking-type photoresist. With increasing conversion ratio of C=C double bonds, the rate of developer intake decreased and the impregnation threshold before the onset of peeling increased and then decreased. It was also found that the dissolution kinetics were affected by the radicals generated upon the decomposition of photoinitiators.

The author performed the pattern formation process mechanism analysis of negative type resists to understand particularly both photocuring process and the dissolution process. Based on the relationship obtained in this thesis between materials constituting negative type resist and the parameters which affect photocuring or development dissolution, the development of high-performance negative type photoresists is expected.

Acknowledgements

The author would like to express her great gratitude to Professor Takahiro Kozawa, the Institute of Scientific and Industrial Research, Osaka University, for his continuous guidance, many invaluable discussion and suggestions, and warm encouragement through this study. The author would like to express her sincere gratitude to research Assistant Sachiyo Uchiyama, Institute of Scientific and Industrial Research, Osaka University, for her continuous guidance, many invaluable discussion and suggestions, and cordial encouragement through this study.

The author is deeply grateful to Professor Shu Seki, and Associate professor Daisuke Sakamaki, Department of Molecular Engineering, Kyoto University, for measurement of quantum efficiency, fruitful discussion and suggestions. The author is also very grateful to Associate Professor Kentaro Taki and Ryouta Hayashi, Chemical and Materials Engineering Course, School of Natural Systems, College of Science and Engineering, Kanazawa University, for Real-time FTIR, fruitful discussion and suggestions. Acknowledgements are also made to Dr. Takayuki Shoda and Qi Gao, Yokohama R&D Center, Mitsubishi Chemical Corporation, for theoretical calculations and valuable discussion.

The author acknowledges to Professor Takashi Hayashi and Professor Hiroshi Uyama, Department of Applied Chemistry, Graduate School of Engineering, Osaka University, for reviewing this thesis and giving their valuable suggestions.

The author wishes to thank all the member of Kozawa Laboratory for their helpful discussion, in especially, Associate Professor Muroya, Kobayashi, Yamamoto and

Okamoto.

Finally, the author expresses great gratitude to her family, Akinori, Ayato, Yukimi, Yasuhiko, Rika, Kana, Chiaki, and Fujiko for their encouragement and many supports.

This study was financially supported by "Dynamic Alliance for Open Innovation Bridging Human, Environment and Materials" from the Ministry of Education, Culture, Sports, Science and Technology of Japan (MEXT), a Grant-in-Aid for Scientific Research (No. JP 261020110, 15K21721, 17H04874, and 26249145) from the Japan Society for the Promotion of Science (JSPS), and Mitsubishi Chemical Corporation.